Chapter 7

Automatic Detection, Tracking, and Sensor Integration

W. G. Bath and G. V. Trunk

The Johns Hopkins University Applied Physics Laboratory

7.1 INTRODUCTION

As digital processing has increased in speed and digital hardware has decreased in cost and size, radars have become more and more automated, so that automatic detection and tracking (ADT) systems are associated with almost all but the simplest of radars.

In this chapter, automatic detection, automatic tracking, and sensor integration techniques for surveillance radars are discussed. Included in the discussion are various noncoherent integrators that provide target enhancement, thresholding techniques for false alarms and target suppression, and algorithms for estimating target position and resolving targets. Then, an overview of the entire tracking system is given, followed by a discussion of its various components such as track initiation, correlation logic, tracking filter, and maneuver-following logic. Finally, the chapter concludes with a discussion of sensor integration and radar netting, including both colocated and multisite systems.

7.2 AUTOMATIC DETECTION

In the 1940s, Marcum[1] applied statistical decision theory to radar and later Swerling[2] extended the work to fluctuating targets. They investigated many of the statistical problems associated with the noncoherent detection of targets in gaussian noise. (Note: If the inphase and quadrature components are gaussian distributed, the envelope is Rayleigh distributed and the power is exponentially distributed.) Marcum's most important result was the generation of curves of probability of detection (P_D) versus signal-to-noise ratio (S/N) for a detector that sums N envelope-detected samples (either linear or square-law) under the assumption of equal signal amplitudes. Whereas for a phased array, the equal amplitude assumption is valid; for a rotating radar, the returned signal amplitude is modulated by the antenna pattern as the beam sweeps over

the target. Many authors have investigated various detectors, comparing detection performance and angular estimation results with optimal values, and many of these results are presented later in this section.

In the original work on detectors, the environment was assumed known and homogeneous, so that fixed thresholds could be used. However, a realistic radar environment (e.g., containing land, sea, and rain) will cause an exorbitant number of false alarms for a fixed-threshold system that does not utilize excellent coherent processing. Three main approaches—adaptive thresholding, nonparametric detectors, and clutter maps—have been used to solve the noncoherent, false-alarm problem. Both adaptive thresholding and nonparametric detectors are based on the assumption that homogeneity exists in a small region about the range cell that is being tested. The adaptive thresholding method assumes that the noise density is known except for a few unknown parameters (e.g., the mean and the variance). The surrounding reference cells are then used to estimate the unknown parameters, and a threshold based on the estimated density is obtained. Nonparametric detectors obtain a constant false-alarm rate (CFAR) by ranking (ordering the samples from smallest to largest) the test sample with the reference cells. Under the hypothesis that all the samples (test and reference) are independent samples from an unknown density function, the rank of the test sample is uniform; and consequently, a threshold that yields CFAR can be set. Clutter maps store an average background level for each range-azimuth cell. A target is then declared in a range-azimuth cell if the new value exceeds the average background level by a specified amount.

Optimal Detector. The radar detection problem is a binary hypothesis-testing problem in which H_0 denotes the hypothesis that no target is present and H_1 is the hypothesis that the target is present. While several criteria (i.e., definitions of optimality) can be used to solve this problem, the most appropriate for radar is the Neyman-Pearson.[3] This criterion maximizes the probability of detection P_D for a given probability of false alarm P_{fa} by comparing the likelihood ratio L (defined by Eq. 7.1) to an appropriate threshold T that determines the P_{fa}. A target is declared present if

$$L(x_1,\ldots,x_n) = \frac{p(x_1,\ldots,x_n|\,H_1)}{p(x_1,\ldots,x_n|\,H_0)} \geq T \tag{7.1}$$

where $p(x_1,\ldots, x_n|H_1)$ and $p(x_1,\ldots, x_n|H_0)$ are the joint probability density functions of the n observations x_i under the conditions of target presence and target absence, respectively. For a linear envelope detector, the samples have a Rayleigh density under H_0 and a Ricean density under H_1, and the likelihood ratio detector reduces to

$$\prod_{i=1}^{n} I_0\left(\frac{A_i x_i}{\sigma^2}\right) \geq T \tag{7.2}$$

where I_0 is the modified Bessel function of zero order, σ^2 is the noise power, and A_i is the target amplitude of the ith pulse and is proportional to the antenna power pattern. For small signals ($A_i << \sigma$), the detector reduces to the square-law detector

$$\sum_{i=1}^{n} A_i^2 x_i^2 \geq T \tag{7.3}$$

and for large signals ($A_i >> \sigma$), it reduces to the linear detector

$$\sum_{i=1}^{n} A_i x_i > T \tag{7.4}$$

For constant signal amplitude (i.e., $A_i = A$), these detectors were first studied by Marcum[1] and were studied in succeeding years by numerous other people. The most important facts concerning these detectors are the following:

- The detection performances of the linear and square-law detectors are similar, differing only by less than 0.2 dB over wide ranges of P_D, P_{fa}, and n.
- Because the signal return of a scanning radar is modulated by the antenna pattern, to maximize the *S/N* when integrating a large number of pulses with no weighting (i.e., $A_i = 1$), only 0.84 of the pulses between the half-power points should be integrated, and the antenna beam-shape factor (ABSF) is 1.6 dB.[4] The ABSF is the number by which the midbeam *S/N* must be reduced so that the detection curves generated for equal signal amplitudes can be used for the scanning radar.
- The collapsing loss for the linear detector can be several decibels greater than the loss for a square-law detector[5] (see Figure 7.1). The collapsing loss is the additional signal required to maintain the same P_D and P_{fa} when unwanted noise samples along with the desired signal-plus-noise samples are integrated. The number of signal samples integrated is N, the number of extraneous noise samples integrated is M, and the collapsing ratio $\rho = (N + M)/N$.
- Most automatic detectors are required not only to detect targets but also to make angular estimates of the azimuth position of the target. Swerling[6] calculated the standard deviation of the optimal estimate by using the Cramer-Rao lower bound. The results

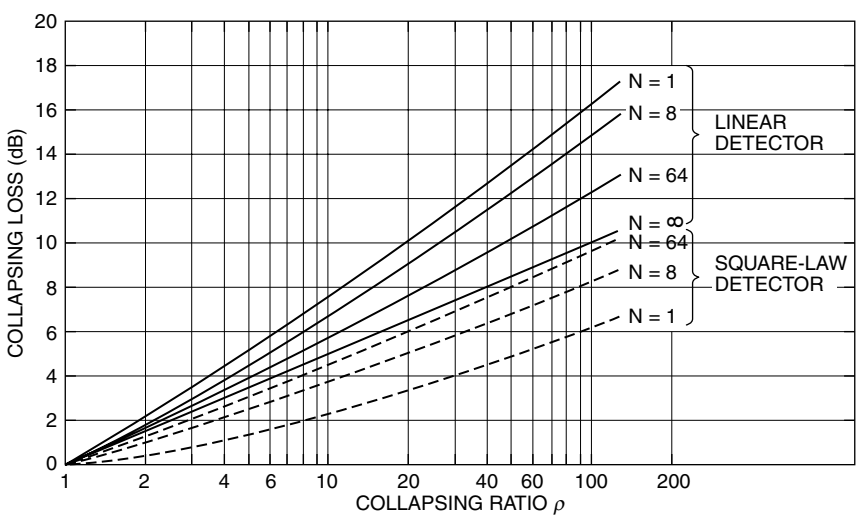

FIGURE 7.1 Collapsing loss versus collapsing ratio for a probability of false alarm of 10^{-6} and a probability of detection of 0.5 (*after G. V. Trunk*[5] *© IEEE 1972*)

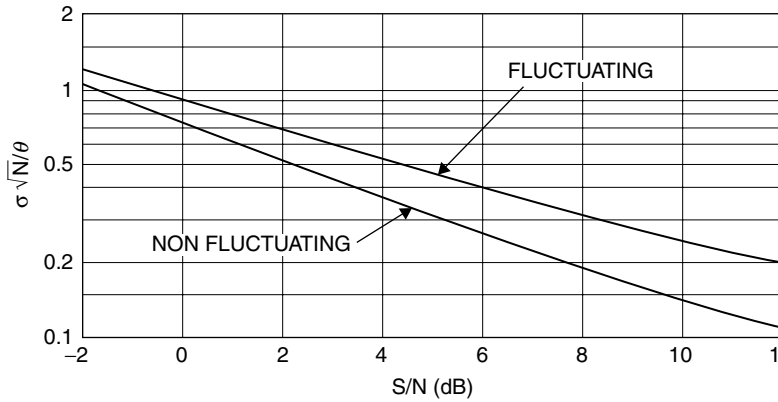

FIGURE 7.2 Cramer-Rao bound for angular estimates for fluctuating and nonfluctuating targets; σ is the standard deviation of the estimation error, and N is the number of pulses within the 3-dB beamwidth, which is θ. The S/N is the value at the center of the beam. (*after P. Swerling*[6] © *IEEE 1956*)

are shown in Figure 7.2, where a normalized standard deviation is plotted against the midbeam S/N. This result holds for a moderate or large number of pulses integrated, and the optimal estimate involves finding the location where the correlation of the returned signal and the derivative of the antenna pattern is zero. Although this estimate is rarely implemented, its performance is approached by simple estimates.

Practical Detectors. Many different detectors (often called *integrators*) are used to accumulate the radar returns as the radar sweeps by a target. A few of the most common detectors[7] are shown in Figure 7.3. The feedback integrator[8,9] and two-pole filter[10,11] are detectors that minimize the data storage requirements. While these detectors may still be found in older radars, they probably would not be implemented in new radars and will not be discussed in this edition. Though all the detectors are shown in Figure 7.3 as being constructed with shift registers, they would normally be implemented with random-access memory. The input to these detectors can be linear video, square-law video, or log video. Because linear video is probably the most commonly used, the advantages and disadvantages of the various detectors will be stated for this video.

Moving Window. The moving window in Figure 7.3*a* performs a running sum of n pulses in each range cell,

$$S_i = S_{i-1} + x_i - x_{i-n} \tag{7.5}$$

where S_i is the sum at the ith pulse of the last n pulses and x_i is the ith pulse. The performance[12] of this detector for $n \approx 10$ is only 0.5 dB worse than the optimal detector given by Eq. 7.3. The detection performance can be obtained by using an ABSF of 1.6 dB and standard detection curves for equal amplitude pulses. The angular estimate that is obtained by either taking the maximum value of the running sum or taking the midpoint between the first and last crossings of the detection threshold has a bias of $n/2$ pulses, which is easily corrected. The standard deviation of the estimation error of both these estimators is about 20 percent higher than the optimal estimate specified

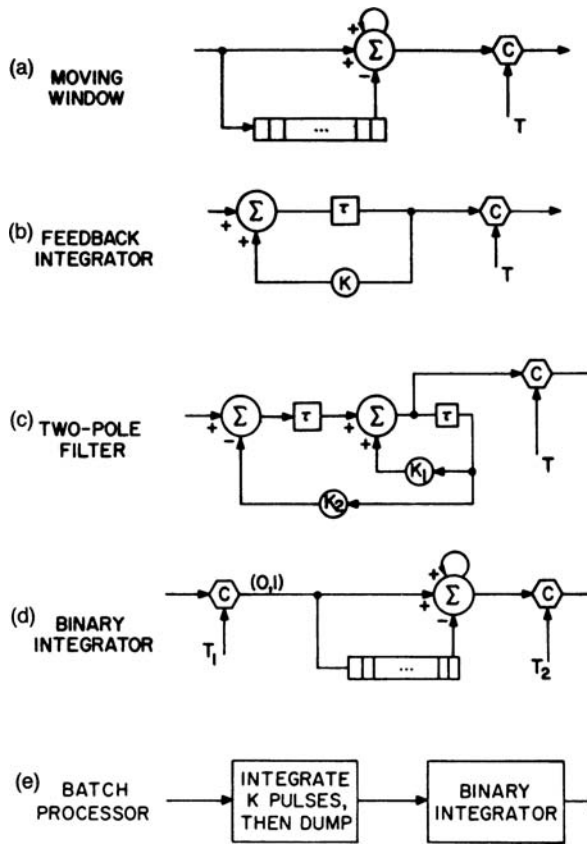

FIGURE 7.3 Block diagrams of various detectors. The letter *C* indicates a comparison, τ is a delay, and loops indicate feedback. (*from G. V. Trunk*[7])

by the Cramer-Rao bound. A disadvantage of this detector is that it is susceptible to interference; that is, one large sample from interference can cause a detection. This problem can be minimized by using soft limiting.

The detection performance discussed previously is based on the assumption that the target is centered in the moving window. In the real situation, the radar scans over the target, and decisions that are highly correlated are made at every pulse. Hansen[13] analyzed this situation for $N = 2$, 4, 8, and 16 pulses and calculated the detection thresholds shown in Figure 7.4, the detection performance shown in Figure 7.5, and the angular accuracy shown in Figure 7.6. Comparing Hansen's scanning calculation with the single-point calculation, one concludes that about 1 dB of improvement is obtained by making a decision at every pulse. The angular error of the beam-splitting procedure is about 20 percent greater than the optimal estimate. For large signal-to-noise ratios, the accuracy (rms error) of the beam-splitting and maximum-return procedures will be limited by the pulse spacing[8] and will approach

$$\sigma(\hat{\theta}) = \Delta\theta/\sqrt{12} \tag{7.6}$$

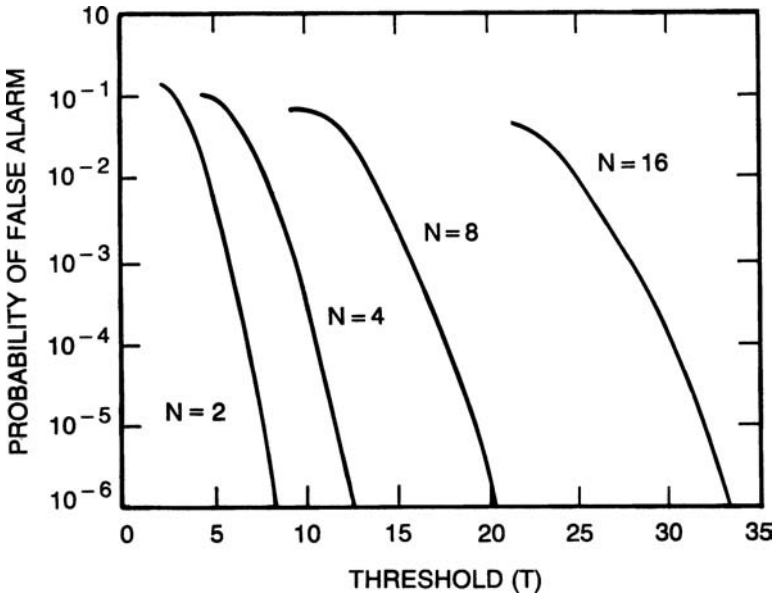

FIGURE 7.4 Single-sweep false-alarm probability P_{fa} versus threshold for moving window. The noise is Rayleigh-distributed with $\sigma = 1$. (*after V. G. Hansen*[13] © *IEEE 1970*)

where $\Delta\theta$ is the angular rotation between transmitted pulses. Consequently, if the number of pulses per beamwidth is small, the angular accuracy will be poor. For instance, if pulses are separated by 0.5 beamwidth, $\sigma(\hat{\theta})$ is bounded by 0.14 beamwidths. However, improved accuracy can be obtained by using the amplitudes of the radar returns. An accurate estimate of the target angle is given by

$$\hat{\theta} = \theta_1 + \frac{\Delta\theta}{2} + \frac{1}{2a\Delta\theta}\ln(A_2/A_1) \tag{7.7}$$

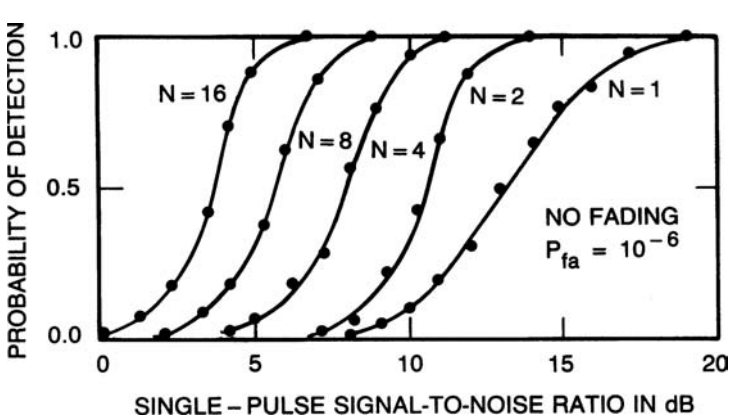

FIGURE 7.5 Detection performance of the analog moving-window detector for the no-fading case (*after V. G. Hansen*[13] © *IEEE 1970*)

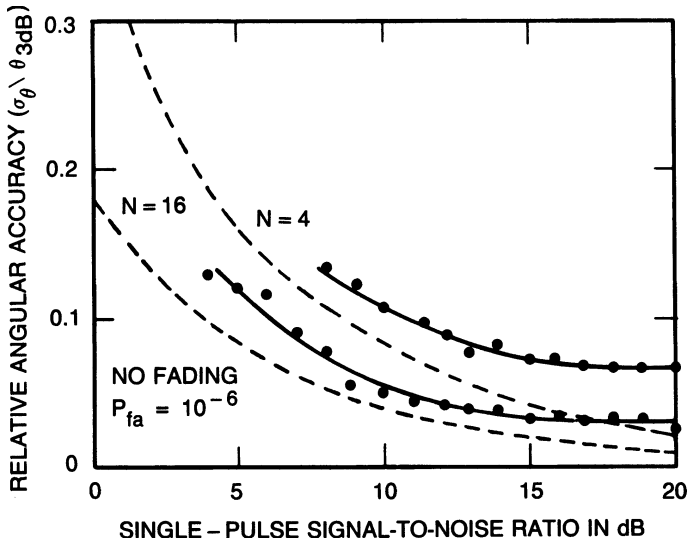

FIGURE 7.6 Angular accuracy obtained with beam-splitting estimation procedure for the no-fading case. Broken-line curves are lower bounds derived by Swerling,[6] and points shown are simulation results. (*after V. G. Hansen*[13] *© IEEE 1970*)

where

$$a = 1.386/(\text{beamwidth})^2 \tag{7.8}$$

and A_1 and A_2 are the two largest amplitudes of the returned samples and occur at angles θ_1 and $\theta_2 = \theta_1 + \Delta\theta$, respectively. Because the estimate should lie between θ_1 and θ_2 and Eq. 7.7 will not always yield such an estimate, $\hat{\theta}$ should be set equal to θ_1 if $\hat{\theta} < \theta_1$ and $\hat{\theta}$ should be equal to θ_2 if $\hat{\theta} > \theta_2$. The accuracy of this estimator is given in Figure 7.7 for the case of $n = 2$ pulses per beamwidth. This estimation procedure can also be used to estimate the elevation angle of a target in multibeam systems where θ_1 and θ_2 are the elevation-pointing angles of adjacent beams and A_1 and A_2 are the corresponding amplitudes.

Binary Integrator. The binary integrator is also known as the dual-threshold detector, M-out-of-N detector, or rank detector (see "Nonparametric Detectors," later in this section), and numerous individuals have studied it.[14–18] As shown in Figure 7.3*d*, the input samples are quantized to 0 or 1, depending on whether or not they are less than a threshold T_1. The last N zeros and ones are summed (with a moving window) and compared with a second threshold $T_2 = M$. For large N, the detection performance of this detector is approximately 2 dB less than the moving-window integrator because of the hard limiting of the data, and the angular estimation error is about 25 percent greater than the Cramer-Rao lower bound. Schwartz[16] showed that within 0.2 dB the optimal value of M for maximum P_D is given by

$$\mathrm{M} = 1.5\sqrt{N} \tag{7.9}$$

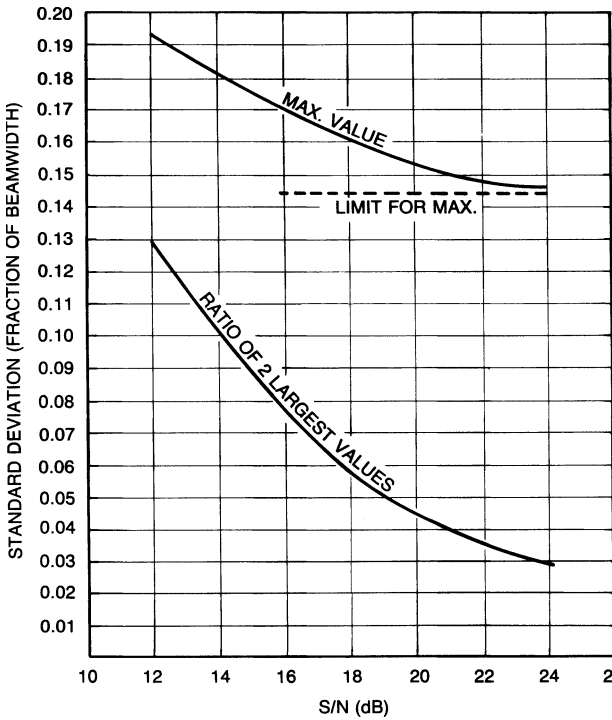

FIGURE 7.7 Angular accuracy for two pulses separated by 0.5 beamwidths

when $10^{-10} < P_{\text{fa}} < 10^{-5}$ and $0.5 < P_D < 0.9$. The optimal value of P_n, the probability of exceeding T_1 when only noise is present, was calculated by Dillard[18] and is shown in Figure 7.8. The corresponding threshold T_1 is

$$T_1 = \sigma(-2 \ln P_N)^{1/2} \tag{7.10}$$

A comparison of the optimal (best value of M) binary integrator with various other procedures is given in Figures 7.9 and 7.10 for $P_D = 0.5$ and 0.9, respectively.

The binary integrator is used in many radars because (1) it is easily implemented; (2) it ignores interference spikes that cause trouble with integrators that directly use signal amplitude; and (3) it works extremely well when the noise has a non-Rayleigh density.[19] For $N = 3$, comparison of the optimal binary integrator (3 out of 3), another binary integrator (2 out of 3), and the moving-window detector in log-normal interference (an example of a non-Rayleigh density, where the log of the return has a gaussian density) is shown in Figure 7.11. The optimal binary integrator is much better than the moving-window integrator. The optimal values for log-normal interference were calculated by Schleher[19] and are $M = 3$, 8, and 25 for $N = 3$, 10, and 30, respectively.

Batch Processor. The batch processor (Figure 7.3*e*) is very useful when a large number of pulses are within the 3-dB beamwidth. If KN pulses are in the 3-dB beamwidth, K pulses are summed (batched) and either a 0 or a 1 is declared, depending on whether or not the batch is less than a threshold T_1. The last N zeros and ones are

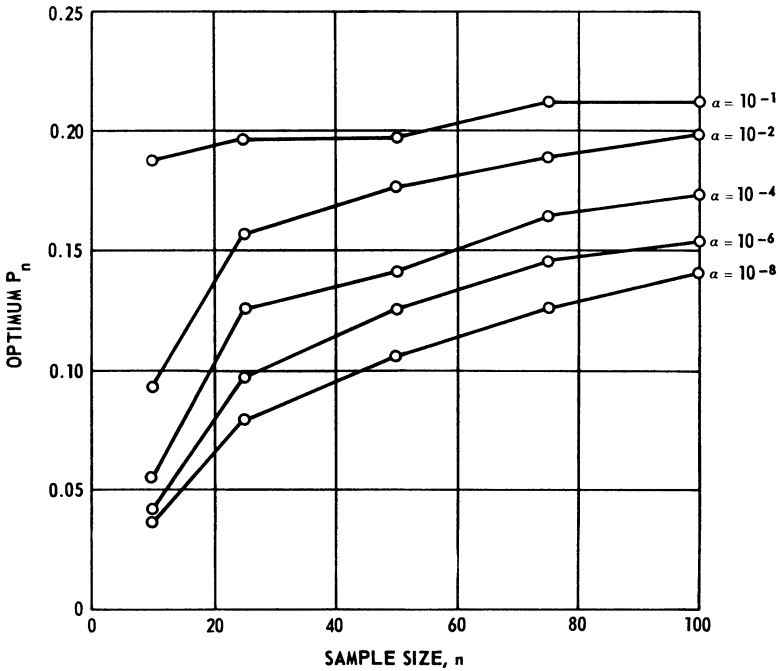

FIGURE 7.8 Optimum values of P_N as a function of the sample size n and the probability of false alarm α; Ricean distribution with $S/N = 0$ dB per pulse. (*after G. M. Dillard*[18] *© IEEE 1967*)

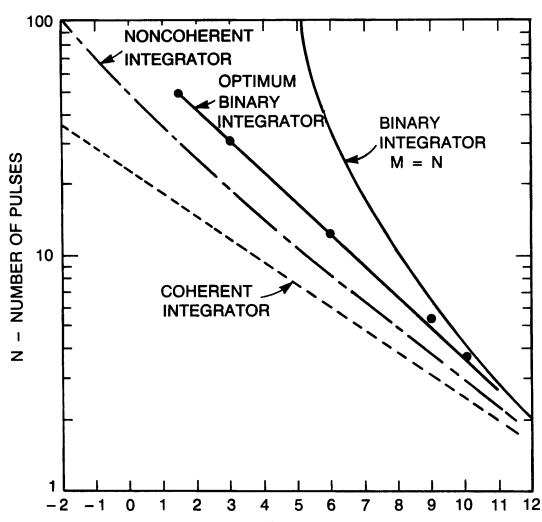

FIGURE 7.9 Comparison of binary integrator (M-out-of-N) with other integration methods ($P_{fa} = 10^{-10}$; $P_D = 0.5$) (*after M. Schwartz*[16] *© IEEE 1956*)

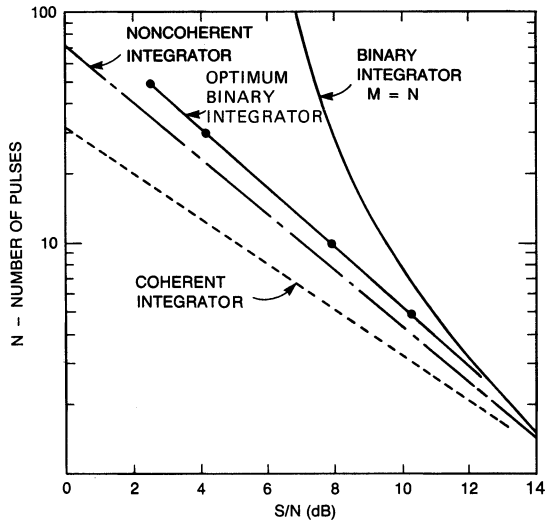

FIGURE 7.10 Comparison of binary integrator (M-out-of-N) with other integration methods ($P_{fa} = 10^{-10}$; $P_D = 0.90$) (*after M. Schwartz*[16] © *IEEE 1956*)

summed and compared with a second threshold M. An alternative version of this detector is to put the batch amplitudes through a moving-window detector.

The batch processor, like the binary integrator, is easily implemented, ignores interference spikes, and works extremely well when the noise has a non-Rayleigh density. Furthermore, the batch processor requires less storage, detects better, and estimates

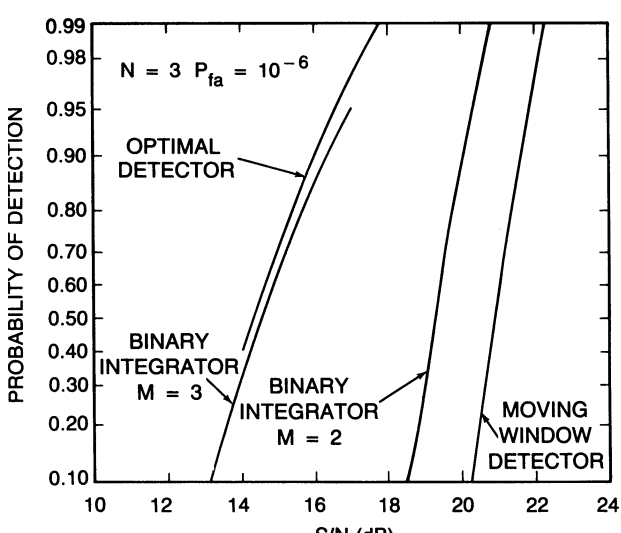

FIGURE 7.11 Comparison of various detectors in log-normal ($\sigma = 6$ dB) interference ($N = 3$; $P_{fa} = 10^{-6}$) (*after D. C. Schleher*[19] © *IEEE 1975*)

angles more accurately than the binary integrator. For instance, if there were 80 pulses on target, one could batch 16 pulses, quantize this result to a 0 or a 1, and declare a target with a 3-out-of-5 (or 2-out-of-5) binary integrator. The detection performance of the batch processor for a large number of pulses integrated is approximately 0.5 dB worse than the moving window. The batch processor has been successfully implemented by the Applied Physics Laboratory[20] of The Johns Hopkins University. To obtain an accurate azimuth estimate $\hat{\theta}$, approximately 20 percent greater than the lower bound,

$$\hat{\theta} = \frac{\sum B_i \theta_i}{\sum B_i} \tag{7.11}$$

is used, where B_i is the batch amplitude and θ_i is the azimuth angle corresponding to the center of the batch.

False-Alarm Control. In the presence of clutter, if fixed thresholds are used with the previously discussed integrators, an enormous number of detections will occur and will saturate and disrupt the tracking computer associated with the radar system. Four important facts should be noted:

- A tracking system should be associated with the automatic detection system (the only exception is when one displays multiple scans of detections).
- The P_{fa} of the detector should be matched to the tracking system to produce the overall lowest *S/N* required to form a track without initiating too many false tracks (see Figure 7.38, later in this chapter).
- Random false alarms and unwanted targets (e.g., stationary targets) are not a problem if they are removed by the tracking system.
- Scan-to-scan processing can be used to remove stationary point clutter or moving-target indication (MTI) clutter residues.

One can limit the number of false alarms with a fixed-threshold system by setting a very high threshold. Unfortunately, this would reduce target sensitivity in regions of low noise (clutter) return. Three main approaches—adaptive threshold, nonparametric detectors, and clutter maps—have been used to reduce the false-alarm problem. Adaptive thresholding and nonparametric detectors assume that the samples in the range cells surrounding the test cell (called *reference cells*) are independent and identically distributed. Furthermore, it is usually assumed that the time samples are independent. Both kinds of detectors test whether the test cell has a return sufficiently larger than the reference cells. Clutter maps allow variation in space, but the clutter must be stationary over several (typically 5 to 10) scans. Clutter maps store an average background level for each range-azimuth cell. A target is then declared in a range-azimuth cell if the new value exceeds the average background level by a specified amount.

Adaptive Thresholding. The basic assumption of the adaptive thresholding technique is that the probability density of the noise is known except for a few unknown parameters. The surrounding reference cells are then used to estimate the unknown parameters, and a threshold based on the estimated parameters is obtained. The simplest adaptive detector, shown in Figure 7.12, is the cell-average CFAR (constant false-alarm rate) investigated by Finn and Johnson.[21] If the noise has a Rayleigh density, $p(x) = x \exp(-x^2/2\sigma^2)/\sigma^2$, only the parameter σ (σ^2 is the noise power) needs to be estimated, and the threshold is of the form $T = K\Sigma x_i = Kn\sqrt{\pi/2}\hat{\sigma}$, where $\hat{\sigma}$ is the

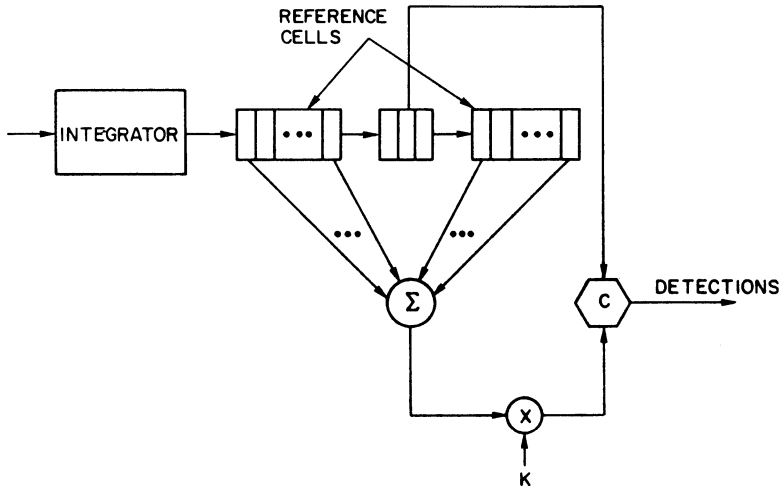

FIGURE 7.12 Cell-averaging CFAR. The letter C indicates a comparison. (*from G. V. Trunk*[7])

estimate of σ. However, since T is set by an estimate $\hat{\sigma}$, it has some error and must be slightly larger than the threshold that one would use if σ were known exactly a priori. The raised threshold causes a loss in target sensitivity and is referred to as a CFAR loss. This loss has been calculated[22] and is summarized in Table 7.1. As can be seen, for a small number of reference cells, the loss is large because of the poor estimate of σ. Consequently, one would prefer to use a large number of reference cells. However, if one does this, the homogeneity assumption (i.e., all the reference cells are statistically similar) might be violated. A good rule of thumb is to use enough reference cells so that the CFAR loss is below 1 dB and at the same time not let the reference cells extend over a range interval that violates the homogenous background assumption. Unfortunately, for a specific radar this might not be feasible.

If there is uncertainty about whether or not the noise is Rayleigh-distributed, it is better to threshold individual pulses and use a binary integrator as shown in Figure 7.13. This detector is tolerant of variations in the noise density because by setting K to yield a 1 with probability 0.1, a $P_{fa} \approx 10^{-6}$ can be obtained by using a 7-out-of-9 detector. While noise may be non-Rayleigh, it will probably be very Rayleigh-like out to the

TABLE 7.1 CFAR Loss for $P_{fa} = 10^{-6}$ and $P_D = 0.9$*

Number of Pulses Integrated	Loss for Various Numbers of Reference Cells (in dB)					
	1	2	3	5	10	∞
1	. . .	. . .	15.3	7.7	3.5	0
3	. . .	7.8	5.1	3.1	1.4	0
10	6.3	3.3	2.2	1.3	0.7	0
30	3.6	2.0	1.4	1.0	0.5	0
100	2.4	1.4	1.0	0.6	0.3	0

*(*after R. L. Mitchell and J. F. Walker*[22] © IEEE 1971)*

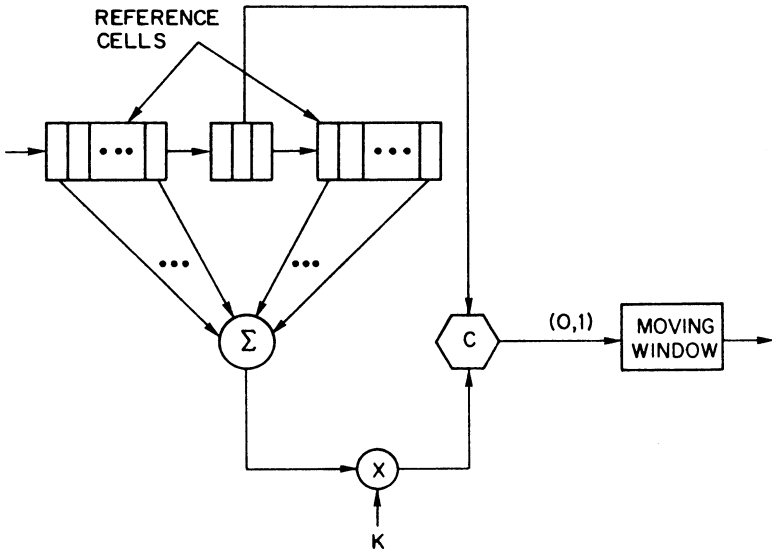

FIGURE 7.13 Implementation of a binary integrator. The letter *C* indicates a comparison. (*from G. V. Trunk*[7])

tenth percentile. Furthermore, one can use feedback based on several scans of data to control K in order to maintain a desired P_{fa} on either a scan or a sector basis. This demonstrates a general rule: to maintain a low P_{fa} in various environments, adaptive thresholding should be placed in front of the integrator.

If the noise power varies from pulse to pulse (as it would in jamming when frequency agility is employed), one must CFAR each pulse and then integrate. While the binary integrator performs this type of CFAR action, analysis[23,24] has verified that the ratio detector shown in Figure 7.14 is a better detector. The ratio detector sums signal-to-noise ratios and is specified by

$$\sum_{i=1}^{n} \frac{x_i^2(j)}{\dfrac{1}{2m}\displaystyle\sum_{k=1}^{m}\left[x_i^2(j+1+k)+x_i^2(j-1-k)\right]} \tag{7.12}$$

where $x_i(j)$ is the ith envelope-detected pulse in the jth range cell and $2m$ is the number of reference cells. The denominator is the maximum-likelihood estimate of σ_i^2, the noise power per pulse. The ratio detector will detect targets even though only a few returned pulses have a high signal-to-noise ratio. Unfortunately, this will also cause the ratio detector to declare false alarms in the presence of narrow-pulse interference. To reduce the number of false alarms when narrow-pulse interference is present, the individual power ratios can be soft-limited[24] to a small enough value so that interference will cause only a few false alarms. A comparison of the ratio detector with other commonly used detectors is shown in Figures 7.15 and 7.16 for nonfluctuating and fluctuating targets. A typical performance in sidelobe jamming when the jamming level varies by 20 dB per pulse is shown in Figure 7.17. By employing a second test to

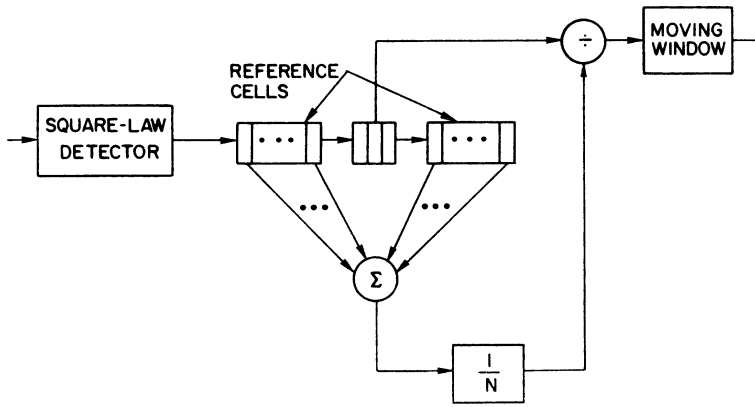

FIGURE 7.14 Ratio detector (*from G. V. Trunk*[7])

identify the presence of narrow-pulse interference, a detection performance approximately halfway between the limiting and nonlimiting ratio detectors can be obtained.

If the noise samples have a non-Rayleigh density such as the chi-square density or log-normal density, it is necessary to estimate more than one parameter and the adaptive detector is more complicated. Usually two parameters are estimated, the mean and the variance, and a threshold of the form $T = \hat{\mu} + K\hat{\sigma}$ is used. The sampled mean is easily obtained. However, the usual estimate of the standard deviation

$$\hat{\sigma} = \left[\frac{1}{N}\Sigma(x_i - \hat{\mu})^2\right]^{1/2} \tag{7.13}$$

where

$$\hat{\mu} = \frac{1}{N}\Sigma x_i \tag{7.14}$$

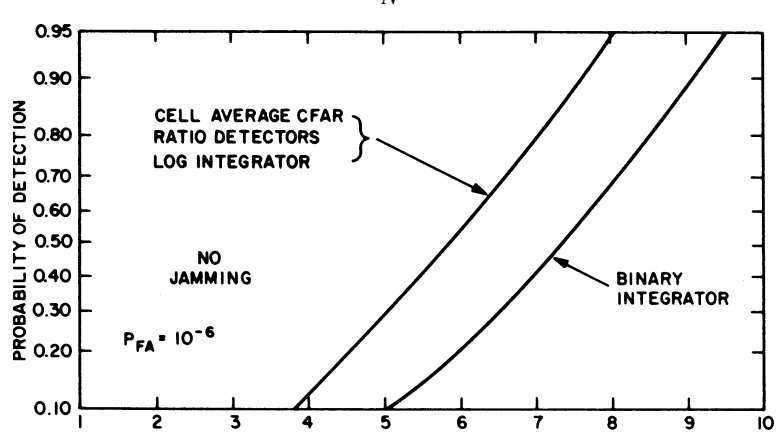

FIGURE 7.15 Curves of probability of detection versus signal-to-noise ratio per pulse for the cell-averaging CFAR, ratio detectors, log integrator, and binary integrator: nonfluctuating target, $N = 6$, $2m = 16$ reference cells, and $P_{fa} = 10^{-6}$ (*from G. V. Trunk and P. K. Hughes*[24])

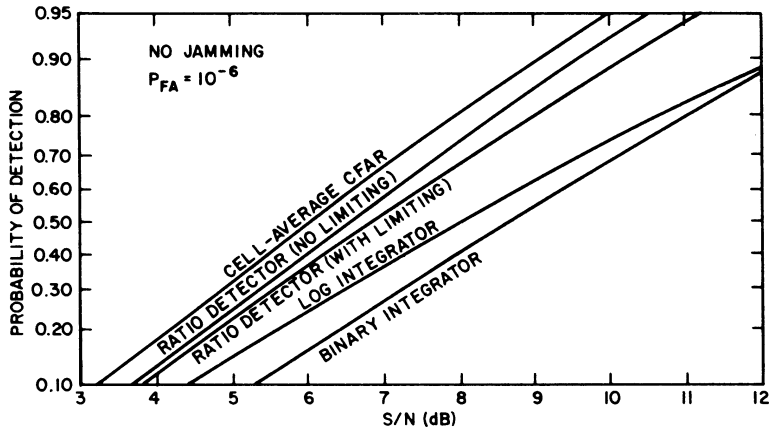

FIGURE 7.16 Curves of probability of detection versus signal-to-noise ratio for the cell-averaging CFAR, ratio detectors, log integrator, and binary integrator: Rayleigh, pulse-to-pulse fluctuating target, $N = 6$, $2m = 16$ reference cells, and $P_{fa} = 10^{-6}$ (*from G. V. Trunk and P. K. Hughes*[24])

is somewhat more difficult to implement; consequently, the mean deviate defined by

$$\sigma = A\sum |x_i - \hat{\mu}| \tag{7.15}$$

is sometimes used because of its ease of implementation and because it is more robust. It should be noted that the CFAR loss associated with a two-parameter threshold is larger than those associated with a one-parameter threshold (see Table 7.1), and for that reason, a two-parameter threshold is rarely used.

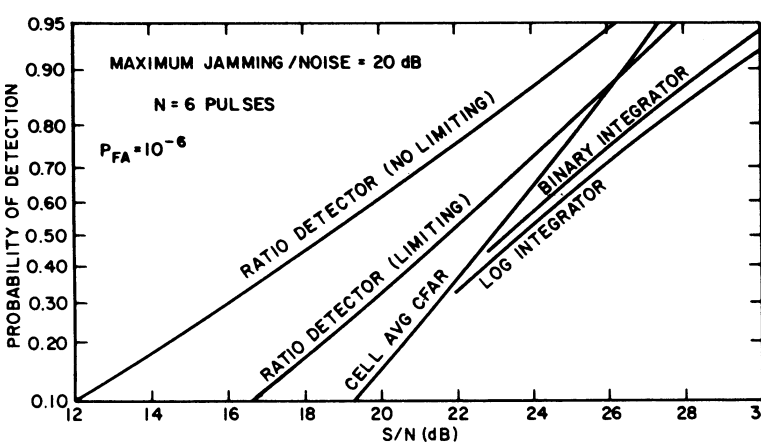

FIGURE 7.17 Curves of probability of detection versus signal-to-noise ratio for the cell-averaging CFAR, ratio detectors, log integrator, and binary integrator: Rayleigh, pulse-to-pulse fluctuations, $2m = 16$ reference cells, $P_{fa} = 10^{-6}$, and maximum jamming-to-noise ratio = 20 dB (*from G. V. Trunk and P. K. Hughes*[24])

If the noise samples are correlated, nothing can be done to the binary integrator to yield a low P_{fa}. Thus, it should not be used in this situation. However, if the correlation time is less than a batching interval, the batch processor will yield a low P_{fa} without modifications.

Target Suppression. Target suppression is the loss in detectability caused by other targets or clutter residues in the reference cells. Basically, there are two approaches to solving this problem: (1) remove large return from the calculation of the threshold[25–27] or (2) diminish the effects of large returns by either limiting or using log video. The technique that should be used is a function of the particular radar system and its environment.

Rickard and Dillard[26] proposed a class of detectors D_K, where the K largest samples are censored (removed) from the reference cells. A comparison of D_0 (no censoring) with D_1 and D_2 for a Swerling 2 target and a single square-law detected pulse is shown in Figure 7.18, where N is the number of reference cells, β is the ratio of the power of the interfering target to the target in the test cell, and the bracketed pair (m, n) indicates the Swerling models of the target and the interfering target, respectively. As shown in Figure 7.18, when one has an interfering target, the P_D does not approach 1 as S/N increases. Another approach[25] that censors samples in the reference cell if they exceed a threshold is briefly discussed in the "Nonparametric Detector" subsection.

Finn[27] investigated the problem of the reference cells spanning two continuous different "noise" fields (e.g., thermal noise, sea clutter, etc.). On the basis of the samples, he estimated the statistical parameters of the two noise fields and the separation point between them. Then, only those reference cells that are in the noise field containing the test cell are used to calculate the adaptive threshold.

An alternative approach for interfering targets is to use log video. By taking the log, large samples in the reference cells will have less effect than linear video on the threshold. The loss associated with using log video, rather than linear video, is 0.5 dB

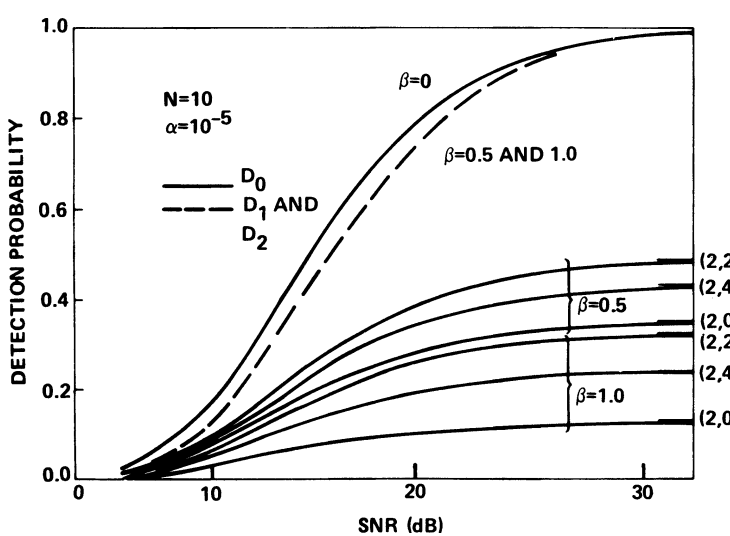

FIGURE 7.18 Detection probability versus SNR for a Swerling Case 2 primary target (*after J. T. Rickard and G. M. Dillard*[26] © *IEEE 1977*)

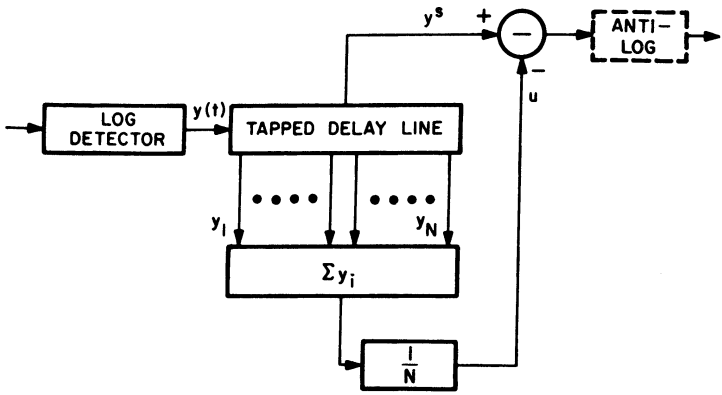

FIGURE 7.19 Block diagram of cell-averaging log-CFAR receiver (*after V. G. Hansen and J. R. Ward*[29] *© IEEE 1972*)

for 10 pulses integrated and 1.0 dB for 100 pulses integrated.[28] An implementation of the log CFAR[29] is shown in Figure 7.19. In many systems, the antilog shown in Figure 7.19 is not taken. To maintain the same CFAR loss as for linear video, the number of reference cells $M_{\log}$ for the log CFAR should equal

$$M_{\log} = 1.65M_{\text{lin}} - 0.65 \tag{7.16}$$

where M_{lin} is the number of reference cells for linear video. The effect of target suppression with log video is discussed later in this section (see Table 7.2, later in the chapter).

Nonparametric Detectors. Usually nonparametric detectors obtain CFAR by ranking the test sample with the reference cells.[30,31] Ranking means that one orders the samples from the smallest to the largest and replaces the smallest with rank 0, the next smallest with rank 1, . . . , and the largest with rank $n - 1$. Under the hypothesis that all the samples are independent samples from an unknown density function, the test sample has equal probability of taking on any of the n values. For instance, referring to the ranker in Figure 7.20, the test cell is compared with 15 of its neighbors. Since, in the set of 16 samples, the test sample has equal probability of being the smallest sample (or equivalently any other rank), the probability that the test sample takes on values 0, 1, . . . , 15 is 1/16. A simple rank detector is constructed by comparing the rank with a threshold K and generating a 1 if the rank is larger, a 0 otherwise. The 0s and 1s are summed in a moving window. This detector incurs a CFAR loss of about 2 dB but achieves a fixed P_{fa} for any unknown noise density as long as the time samples are independent. This detector was incorporated into the ARTS-3A postprocessor used in conjunction with the Federal Aviation Administration airport surveillance radar (ASR). The major shortcoming of this detector is that it is fairly susceptible to target suppression (e.g., if a large target is in the reference cells, the test cell cannot receive the highest ranks).

If the time samples are correlated, the rank detector will not yield CFAR. A modified rank detector, called the modified generalized sign test (MGST),[25] maintains a low P_{fa} and is shown in Figure 7.21. This detector can be divided into three parts: a ranker, an integrator (in this case, a two-pole filter), and a threshold (decision process). A target is declared when the integrated output exceeds two thresholds.

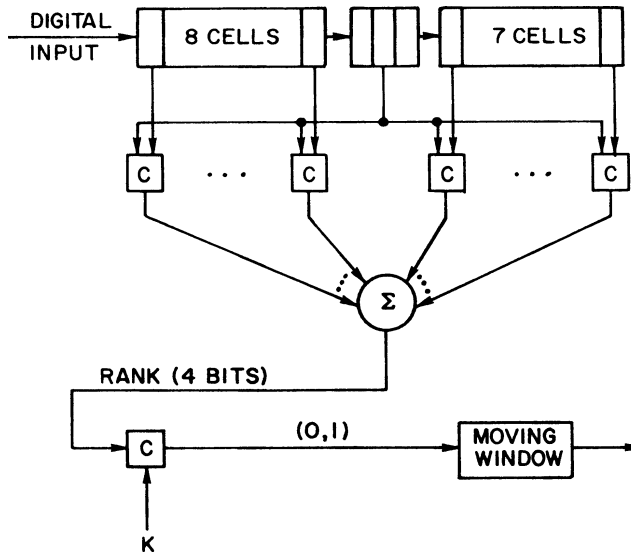

FIGURE 7.20 Rank detector: output of a comparator C is either a zero or a one (*from G. V. Trunk*[7])

The first threshold is fixed (equals $\mu + T_1/K$ in Figure 7.21) and yields $P_{fa} = 10^{-6}$ when the reference cells are independent and identically distributed. The second threshold is adaptive and maintains a low P_{fa} when the reference samples are correlated. The device estimates the standard deviation of the correlated samples with the mean deviate estimator, where extraneous targets in the reference cells have been excluded from the estimate by use of a preliminary threshold T_2.

The basic disadvantages of all nonparametric detectors are that (1) they have relatively large CFAR losses; (2) they have problems with correlated samples; and (3) one loses amplitude information, which can be a very important discriminant between target and clutter.[32] For example, a large return (*cross section* ≥ 1000 m^2) in a clutter area is probably just clutter breakthrough. See "Radar Detection Acceptance" in Section 7.3.

Clutter Mapping. A clutter map uses adaptive thresholding where the threshold is calculated from the return in the test cell on previous scans rather than from the surrounding reference cells on the same scan. This technique has the advantage in that for essentially stationary environments (e.g., land-based radar against ground clutter), the radar has interclutter visibility—it can see between large clutter returns. Lincoln Laboratory[33] in its moving-target detector (MTD) used a clutter map for the zero-doppler filter very effectively. The decision threshold T for the ith cell is

$$T = A\ S_{i-1} \tag{7.17}$$

where the clutter is estimated using a simple feedback integrator

$$S_i = K\ S_{i-1} + X_i \tag{7.18}$$

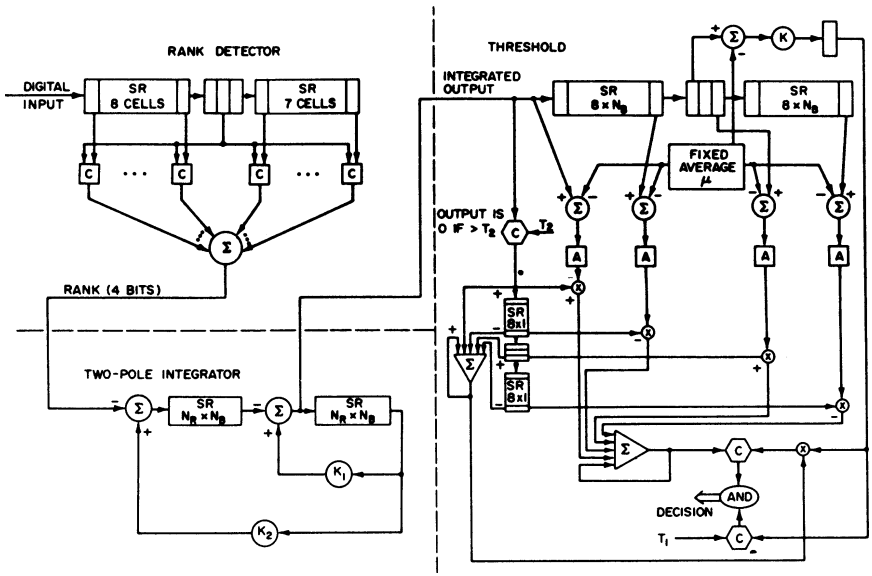

FIGURE 7.21 Modified generalized sign test processor (*after G. V. Trunk et al.*[25] *1974*)

where S_i is the average background level, X_i is the return in the ith cell, K is the feedback value that determines the map time constant, and A is the constant that determines the P_{fa}. In the MTD used for the ASR application, K is 7/8, which effectively averages the last eight scans. The purpose of the clutter map is to detect, in clutter free areas, crossing targets that would have been removed by the doppler processing. The main utility of clutter maps is with fixed-frequency, land-based radars. While clutter maps can be used with frequency-agile radars and on moving platforms (e.g., radars on ships), they are not nearly as effective in these environments.

Target Resolution. In automatic detection systems, a single large target will probably be detected (i.e., cross a detection threshold) many times, e.g., in adjacent range cells, azimuth beams, and elevation beams. Therefore, automatic detection systems have algorithms for merging the individual detections into a single centroided detection. Most algorithms have been designed so that they will rarely split a single target into two targets. This procedure results in poor range resolution capability. A merging algorithm[34] often used is the adjacent-detection merging algorithm, which decides whether a new detection is adjacent to any of the previously determined sets of adjacent detections. If the new detection is adjacent to any detection in the set of adjacent detections, it is added to the set. Two detections are adjacent if two of their three parameters (range, azimuth, and elevation) are the same and the other parameter differs by the resolution element: range cell ΔR, azimuth beamwidth θ, or elevation beamwidth γ.

A study[34] compared the resolving capability of three common detection procedures: linear detector with $T = \hat{\mu} + A\hat{\sigma}$, linear detector with $T = B\hat{\mu}$, and log detector with $T = C + \hat{\mu}$, where the constants A, B, and C are used to obtain the same P_{fa} for all detectors. The estimates $\hat{\mu}$ and $\hat{\sigma}$ of μ and σ were obtained from either (1) all the reference cells or (2) the leading or lagging half of the reference cells, choosing the

TABLE 7.2 Probability of Detecting Both Targets with Log Video When the Two Targets Are Separated by 1.5, 2.0, 2.5, or 3.0 Range Cells (*S/N* of target 1 is 20 dB and *S/N* of target 2 is 10, 13, 20, 30, or 40 dB)*

Thresholding Technique	Target Separation	S/N of Target no. 2				
		10	13	20	30	40
All reference cells	1.5	0.00	0.04	0.00	0.00	0.00
	2.0	0.00	0.22	0.54	0.14	0.10
	2.5	0.04	0.24	0.94	0.62	0.32
	3.0	0.00	0.24	0.88	0.92	0.78
Reference cells with minimum mean value	1.5	0.00	0.00	0.00	0.00	0.02
	2.0	0.10	0.32	0.44	0.12	0.04
	2.5	0.18	0.58	0.98	0.46	0.28
	3.0	0.22	0.66	0.98	0.82	0.74

*(*after G. V. Trunk*[34] © *IEEE 1978*)

half with the lower mean value. The first simulation involved two targets separated by 1.5, 2.0, 2.5, or 3.0 range cells and a third target 7.0 range cells from the first target. When the two closely spaced targets were well separated, either 2.5 or 3.0 range cells apart, the probability of detecting both targets (P_{D2}) was < 0.05 for the linear detector with $T = \hat{\mu} + A\hat{\sigma}$; $0.15 < P_{D2} < 0.75$ for the linear detector with $T = B\hat{\mu}$; and $P_{D2} > 0.9$ for the log detector. A second simulation, involving only two targets, investigated the effect of target suppression on log video, and the results are summarized in Table 7.2. The maximum value of P_{D2} is obtained when both targets have an *S/N* of 20 dB. If one of the targets has a larger *S/N* than the other target, suppression occurs—either target 1 suppresses target 2 or vice versa. Also, one notes an improved performance for a small *S/N* (10 to 13 dB) when calculating the threshold using only the half of the reference cells with the lower mean value. The resolution capability of the log detector that uses only the half of the reference cells with the lower mean is shown in Figure 7.22. The probability of resolving two, equal-amplitude targets does not rise above 0.9 until they are separated in range by 2.5 pulse widths.

By assuming that the target is small with respect to the pulse width and that the pulse shape is known, the resolution capability can be improved by fitting the known pulse shape to the received data and comparing the residue square error with a threshold.[35] If only one target is present, the residue should be only noise and hence should be small. If two or more targets are present, the residue will contain signal from the remaining targets and should be large. The results of resolving two targets with *S/N* = 20 dB are shown in Figure 7.23. These targets can be resolved at a resolution probability of 0.9 with a false alarm probability of 0.01 at separations varying between one-fourth and three-fourths of a pulse width, depending on the relative phase difference between the two targets. Moreover, this result can be improved further by processing multiple pulses.

Automatic Detection Summary. When only 2 to 4 samples (pulses) are available, a binary integrator should be used to avoid false alarms due to interference. When a moderate number of pulses (5 to 16) are available, a binary integrator or a moving-window integrator should be used. If the number of pulses is large (greater than 20), a batch processor should be used. If the samples are independent, a one-parameter (mean) threshold can be used. If the samples are dependent, one can either use

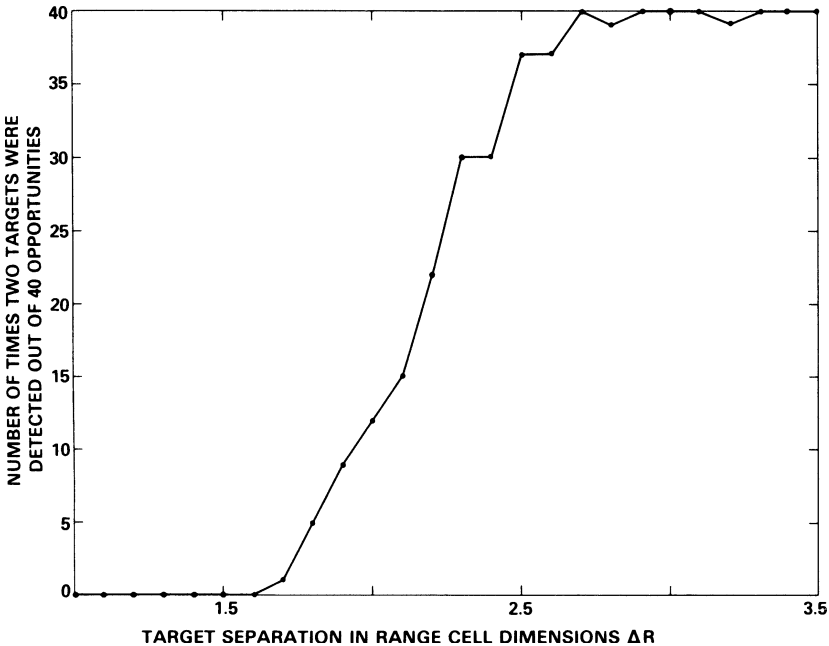

FIGURE 7.22 Resolution capability of a log detector that used half of the references cells with lower mean (*after G. V. Trunk*[34] *© IEEE 1978*)

a two-parameter (mean and variance) threshold or adapt a one-parameter threshold on a sector basis. However, these rules should serve only as a general guideline. It is *highly recommended* that before a detector is chosen the radar video from the environment of interest be collected and analyzed and that various detection processes be simulated on a computer and tested against the recorded data.

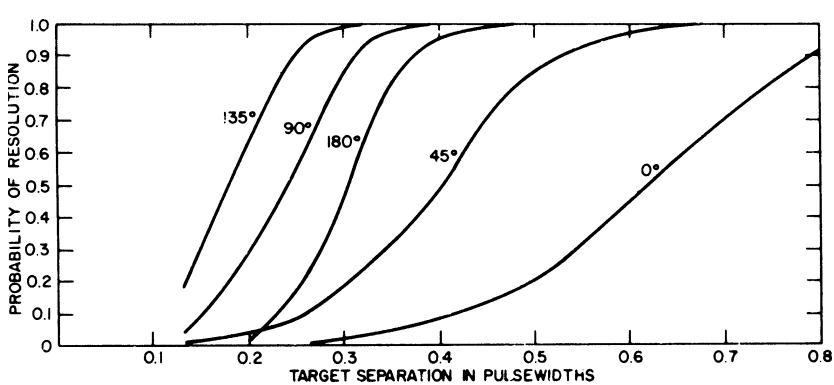

FIGURE 7.23 Probability of resolution as a function of range separation: probability of false alarm is 0.01; sampling rate ΔR = 1.5 samples per pulse width; target strengths, nonfluctuating, A1 = A2 = 20 dB; phase differences = 0°, 45°, 90°, 135°, and 180°. (*after G. V. Trunk*[35] *© IEEE 1984*)

Many modern radars use coherent processing to remove clutter. For the purpose of applying the previous discussions on noncoherent processing to coherent processing, the integrated output in a range-doppler cell of the doppler processor for a single coherent processing interval (CPI) can be treated as a single noncoherent pulse. Because three ambiguous measurements (i.e., detections) are usually required to remove the range and doppler ambiguities,[36,37] 4 to 8 CPIs may be transmitted, and hence, there are usually 4 to 8 noncoherent pulses available for processing.

7.3 AUTOMATIC TRACKING

A track represents the belief that a physical object or "target" is present and has actually been detected by the radar. An automatic radar tracking system forms a track when enough radar detections are made in a believable enough pattern to indicate a target is actually present (as opposed to a succession of false alarms) and when enough time has passed to allow accurate calculation of the target's kinematic state—usually position and velocity. Thus, the goal of tracking is to transform a (time-lapse) detection picture (shown in Figure 7.24*a*), consisting of target detections, false alarms, and clutter, into a track picture (shown in Figure 7.24*b*), consisting of tracks on real targets, occasional false tracks, and occasional deviations of track position from true target positions.

Figures 7.24*a* and 7.24*b* also illustrate some of the challenges of automatic tracking. Detections are made on targets, but some detections are missing because of target fades or multiple targets in the same resolution cell, whereas additional detections are present due to clutter or noise.

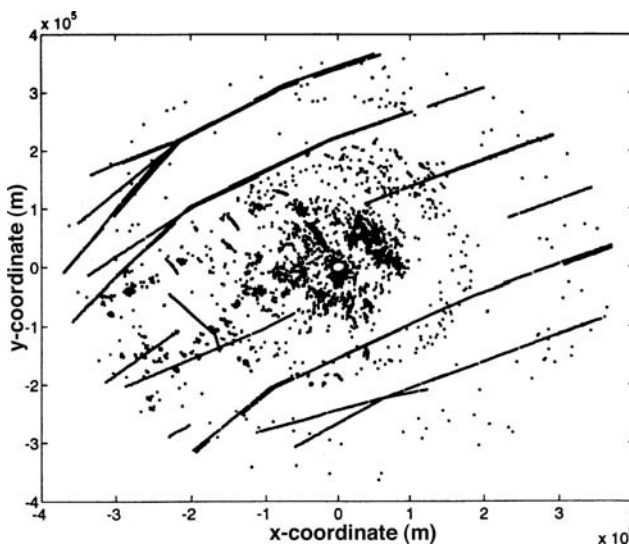

FIGURE 7.24*a* Thirty-minute time lapse of AN/FPN-504 (L band) air traffic control radar detections over a ±400-km square area (*after H. Leung et al.*[38] © *IEEE 1999*)

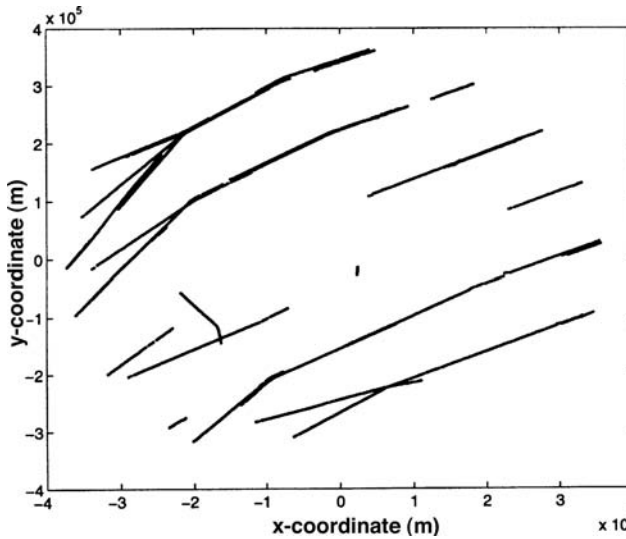

FIGURE 7.24*b* Thirty-minute time lapse of tracks formed from data in Figure 7.24*a*, using Global Nearest-Neighbor (GNN) Technique (*after H. Leung et al.*[38] *© IEEE 1999*)

Automatic tracking can generally be divided into the five steps shown in Figure 7.25 and detailed here:

1. Radar detection acceptance: accepting or rejecting detections for insertion into the tracking process. The purpose of this step is to control false track rates.
2. Association of accepted detections with existing tracks.
3. Updating existing tracks with associated detections.
4. New track formation using unassociated detections.
5. Radar scheduling and control.

The result of the automatic tracking process is a track file that contains a track state for each target detected by the radar.

As shown in Figure 7.25, there is a feedback loop between all these functions so the ability to update existing tracks accurately naturally affects the ability to associate detections with existing tracks. Also, the ability to correctly associate detections with existing tracks affects the track's accuracy and the ability to correctly distinguish between an existing track and a new one. The detection accept/reject step makes use of feedback from the association function that measures the detection activity in different regions of the radar coverage. More stringent acceptance criteria are applied in more active regions.

Track File. When a track is established in the computer, it is assigned a track number. All parameters associated with a given track are referred to by this track number. Typical track parameters are the filtered and predicted position; velocity; acceleration (when applicable); time of last update; track quality; signal-to-noise ratio; covariance matrices (the covariance contains the accuracy of all the track coordinates and all the statistical cross-correlations between them), if a Kalman-type filter is being used; and

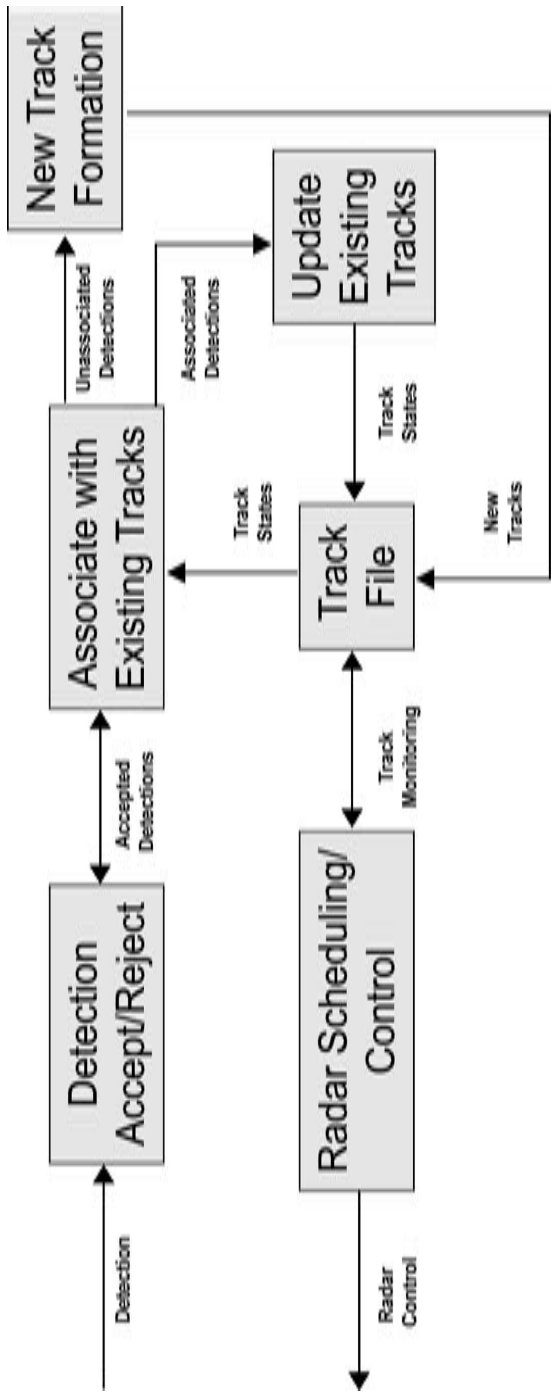

FIGURE 7.25 Structure of automatic tracking process

track history (i.e., the last *n* detections). Tracks and detections can be accessed in various sectored, linked-list, and other data structures so that the association process can be performed efficiently.[39] In addition to the track file, a clutter file is maintained. A clutter number is assigned to each stationary or very slowly moving echo. All parameters associated with a clutter point are referred to by this clutter number. Again, each clutter number is assigned to a sector in azimuth for efficient association.

Radar Detection Acceptance. When the radar system has either no or limited coherent processing, not all the detections declared by the automatic detector are used in the tracking process. Rather, many of the detections (contacts) are filtered out in software using a process called *activity control.*[32,40] The basic idea is to use detection signal characteristics in connection with a map of the detection activity to reduce the rate of detections to one that is acceptable for forming tracks. The map is constructed by counting the unassociated detections (those that do not associate with existing tracks) at the point in the track processing shown in Figure 7.25.

Counts are averaged over many revisits of the radar to achieve statistical significance. The detection signal characteristics (such as amplitude or signal-to-noise) are then re-thresholded to reduce sensitivity in regions of unacceptably high activity. In no circumstances are detections eliminated if they fall within a track gate (i.e., a gate centered on the predicted position of a firm track). Figure 7.26 illustrates an example

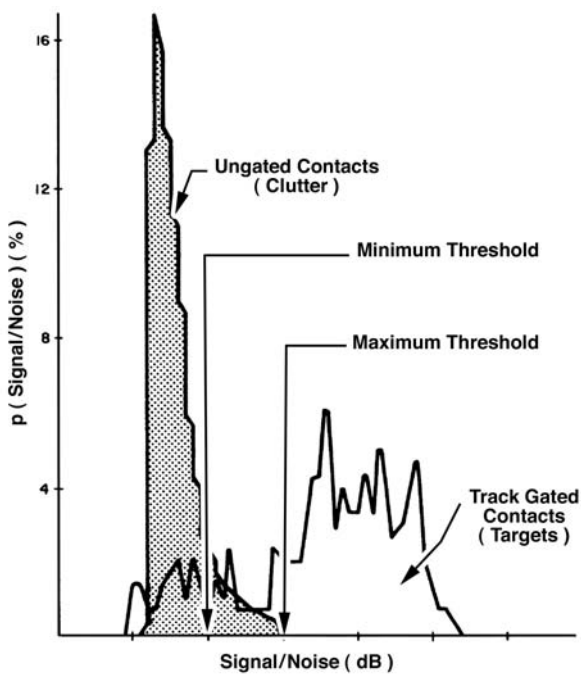

FIGURE 7.26 Histogram of detection signal-to noise ratio detection illustrating the effectiveness of the activity control using the signal-to-noise test in rain clutter. Ungated contacts generally represent clutter. Gated contacts generally represent targets. Re-thresholding, in this case, successfully eliminates large numbers of clutter detections while preserving most target detections. (*after W. G. Bath et al.*[32])

of this process when large numbers of rain clutter detections are potentially overloading the tracking process. In this case, activity control effectively eliminates most of the clutter detections without eliminating many of the actual target detections. However, because this process essentially constitutes controlled desensitization of the radar, it must be used with care. The mapping of the detection activity must be precise so that desensitization occurs only in those regions requiring it.

Updating Existing Tracks with Associated Detections. The simplest method of updating a track state is the α-β filter[41] described by

$$x_s(k) = x_p(k) + \alpha[x_m(k) - x_p(k)] \tag{7.19}$$

$$v_s(k) = v_s(k-1) + \beta[x_m(k) - x_p(k)]/T \tag{7.20}$$

$$x_p(k+1) = x_s(k) + v_s(k)T \tag{7.21}$$

where $x_s(k)$ is the filtered position, $v_s(k)$ is the filtered velocity, $x_p(k)$ is the predicted position, $x_m(k)$ is the measured position, T is the time between detections, and (α, β) are the position and velocity gains, respectively. The selection of (α, β) is a design tradeoff. Small gains make a small correction in the direction of each detection. As a result, the tracking filter is less sensitive to noise but is more sluggish to respond to maneuvers—deviation from the assumed target model. Conversely, large gains produce more tracking noise but quicker response to maneuvers. These errors are readily calculated as a function of α and β using the formulas shown in Table 7.3.

To tune the α-β filter for radar tracking, one uses the radar parameters to calculate the tracking errors listed in Table 7.3 as a function of the tracking gains α and β. Then one selects the gains that best meet the needs of the application. For example, consider a radar that has 50-meter range measurement accuracy and a two-second constant update interval. The application of this radar system is to track a target that moves linearly but with occasional unpredictable maneuvers of up to 1 g (9.8 m/s^2).

TABLE 7.3 Characterization of Tracking Errors as a Function of Tracking Gains α and β

Error Source	Steady-state Track Error	In Position	In Velocity
Radar detection noise (standard deviation- σ)	Standard deviation of filtered tracking state	$\sigma\left[\frac{2\alpha^2+\beta(2-3\alpha)}{\alpha([4-2\alpha-\beta])}\right]^{1/2}$	$\frac{\sigma}{T}\times\left[\frac{2\beta^2}{\alpha[4-2\alpha-\beta]}\right]^{1/2}$
Radar detection noise (standard deviation- σ)	Standard deviation of predicted tracking state	$\sigma\left[\frac{2\alpha^2+\alpha\beta+2\beta}{\alpha([4-2\alpha-\beta])}\right]^{1/2}$	$\frac{\sigma}{T}\times\left[\frac{2\beta^2}{\alpha[4-2\alpha-\beta]}\right]^{1/2}$
Constant maneuver—a (units of g's)	Lag (bias) in filtered track state	$aT^2\frac{(1-\alpha)}{\beta}$	$aT\left(\frac{\alpha}{\beta}-\frac{1}{2}\right)$
Constant maneuver—a (units of g's)	Lag (bias) in predicted track state	$\frac{aT^2}{\beta}$	$aT\left(\frac{\alpha}{\beta}+\frac{1}{2}\right)$

For simplicity, assume the Benedict-Bordner constant relationship[41] [$\beta = \alpha^2/(2 - \alpha)$] between α and β.

The position accuracy of the filter can then be calculated using the formulas in Table 7.3 and is shown in Figure 7.27. When the target is nonmaneuvering, accuracy, as measured by the standard deviation of the predicted tracking state, improves monotonically as the tracking gain α decreases to 0. Conversely, when the target is performing the 1-g maneuver, accuracy, as measured by the lag (or bias) in the predicted tracking state, improves monotonically as the tracking gain increases to 1. The total tracking error can be defined as the error that is exceeded only 1% of the time due to the sum of random errors and bias. The total range-tracking error is best in the region $0.6 < \alpha < 0.9$ with a minimum around 0.75. If accuracy for maneuvers is the dominant concern, then one would probably tune this filter to 0.75 to achieve the lowest total error for a 1-g acceleration. This same technique can be applied to many different radar-tracking problems using the equations in Table 7.3 to calculate a graph such as the one shown in Figure 7.27.

For simple tracking problems, the α-β filter with constant gains selected for the application will often be adequate. However, more complex tracking problems require variable tracking gains (e.g., larger gains at the beginning of the track and larger gains after missed detections or when the range to the track decreases, making angle noise less of an issue). A systematic method for calculating the gains depending on the situation is the

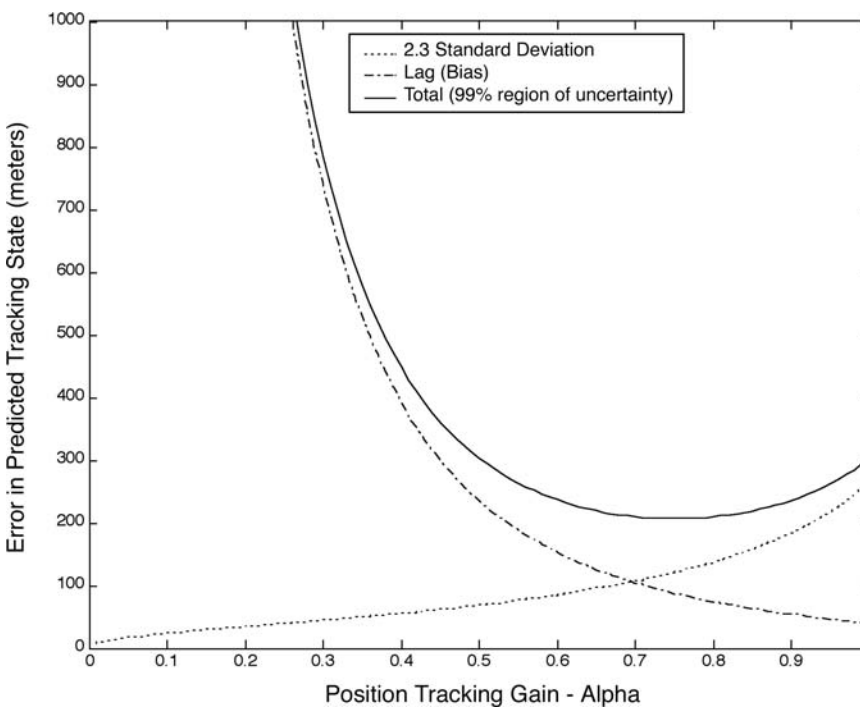

FIGURE 7.27 Example of the tuning of an α-β radar range-tracking filter by selecting the gain that minimizes total error (radar parameters: range accuracy, 50 meters; update interval, 2 seconds; target parameter, 1 g unknown acceleration; gain relation, [$\beta = \alpha^2/(2 - \alpha)$])

Kalman filter.[42,43] The Kalman filter minimizes the mean-square prediction error when the random processes are gaussian. The Kalman filter can be formulated for target motion in one, two, or three dimensions in polar, Cartesian, or Earth-centered coordinates and for three-dimensional, two-dimensional, or one-dimensional radar measurements. For simplicity, a three-dimensional tracking problem in Cartesian space with three measured radar dimensions is considered here. Target motion is described by

$$X(t_{k+1}) = \phi(t_k)\, X(t_k) + A(t_k) + A_p(t_k) \tag{7.22}$$

where $X(t_k)$ is the target state at time t_k, consisting of position and velocity components; $\phi(t_k)$ is a transition matrix that moves the target linearly over an elapsed time, $T_k = t_{k+1} - t_k$, from time t_k to time t_{k+1}; $A(t_k)$ is the target state change due to an unknown acceleration caused by a maneuver or atmospheric drag; and $A_p(t_k)$ is target state change due to a known acceleration that can be corrected, such as gravity for a falling object or Coriollis acceleration. The components of the state vector and transition matrix for this problem are[44]

$$X(t_k) = \begin{vmatrix} x(t_k) \\ \dot{x}(t_k) \\ y(t_k) \\ \dot{y}(t_k) \\ z(t_k) \\ \dot{z}(t_k) \end{vmatrix} \qquad \phi(t_k) = \begin{vmatrix} 1 & T_k & 0 & 0 & 0 & 0 \\ 0 & 1 & 0 & 0 & 0 & 0 \\ 0 & 0 & 1 & T_k & 0 & 0 \\ 0 & 0 & 0 & 1 & 0 & 0 \\ 0 & 0 & 0 & 0 & 1 & T_k \\ 0 & 0 & 0 & 0 & 0 & 1 \end{vmatrix} \tag{7.23}$$

The unknown acceleration $A(t_k)$ is zero-mean and is characterized by its covariance matrix $Q(t_k)$. If one views the unknown maneuver as a white-noise process with spectral density q g/Hz, then the acceleration is sampled by each radar detection producing a discrete covariance matrix:

$$Q(t_k) = q \begin{vmatrix} T_k^3/3 & T_k^2/2 & 0 & 0 & 0 & 0 \\ T_k^2/2 & T_k & 0 & 0 & 0 & 0 \\ 0 & 0 & T_k^3/3 & T_k^2/2 & 0 & 0 \\ 0 & 0 & T_k^2/2 & T_k & 0 & 0 \\ 0 & 0 & 0 & 0 & T_k^3/3 & T_k^2/2 \\ 0 & 0 & 0 & 0 & T_k^2/2 & T_k \end{vmatrix} \tag{7.24}$$

The observation equation relates the actual radar measurements Y_k at time t_k to the target state

$$Y_k = h(X(t_k)) + n_k \tag{7.25}$$

where n_k is the radar measurement noise having a covariance matrix

$$\Re_k = \begin{vmatrix} \sigma_r^2 & 0 & 0 & 0 \\ 0 & \sigma_\theta^2 & 0 & 0 \\ 0 & 0 & \sigma_\varphi^2 & 0 \\ 0 & 0 & 0 & \sigma_D^2 \end{vmatrix} \tag{7.26}$$

composed of the radar measurement accuracies in range, azimuth, elevation, and doppler. The function h is the coordinate transform that relates the measurements to the state at time t_k according to the coordinate frame design choices (see Table 7.5, later in the chapter). In order to use the Kalman filter, h is approximated as a linear function in the vicinity of the predicted track state

$$h(X) = h(\hat{X}(t_{k+1} \mid t_k) + H[X - \hat{X}(t_{k+1} \mid t_k)] \times (X - \hat{X}(t_{k+1} \mid t_k) \tag{7.27}$$

where H is the gradient of h. Each coordinate frame has its own approximation for H. For example, if the state coordinate system is composed of three-dimensional Cartesian coordinates centered at the radar, then multiplication by H transforms Cartesian coordinates (x, y, z) into polar measurement coordinates (range, azimuth, elevation, doppler) and

$$H = \begin{bmatrix} \frac{x}{r} & \frac{y}{r} & \frac{z}{r} & 0 & 0 & 0 \\ \frac{y}{x^2+y^2} & \frac{-x}{x^2+y^2} & 0 & 0 & 0 & 0 \\ \frac{-xz}{r^2\sqrt{x^2+y^2}} & \frac{-yz}{r^2\sqrt{x^2+y^2}} & \frac{\sqrt{x^2+y^2}}{r^2} & 0 & 0 & 0 \\ \frac{\dot{x}r - x\dot{r}}{r^2} & \frac{\dot{y}r - y\dot{r}}{r^2} & \frac{\dot{z}r - z\dot{r}}{r^2} & \frac{x}{r} & \frac{y}{r} & \frac{z}{r} \end{bmatrix} \tag{7.28}$$

where $r = \sqrt{x^2 + y^2 + z^2}$ is range.

The Kalman filter equations for radar tracking are then, simply, generalizations of the $\alpha - \beta$ filter equations where α and β vary with time. The Kalman filter update procedure continues as follows.

First, predict a new target state estimate $\hat{X}(t_{k+1} \mid t_k)$ of the state $X(t_{k+1})$ at time t_{k+1} given all measurements up to time t_k

$$\hat{X}(t_{k+1} \mid t_k) = \phi(t_k)X(t_k) + A_p(t_k) \tag{7.29}$$

along with its covariance

$$P(k+1 \mid k) = \phi(t_k)P(k \mid k)\phi(t_k)^T + Q(t_k) \tag{7.30}$$

Then, update the target state using the $(k + 1)$st radar measurement

$$\hat{X}(t_{k+1} \mid t_{k+1}) = \hat{X}(t_{k+1} \mid t_k) + K_k[Y_{k+1} - H(t_{k+1})\hat{X}(t_{k+1} \mid t_k)] \tag{7.31}$$

and its covariance

$$P(k+1 \mid k+1) = [I - K_{k+1}H(t_{k+1})]P(k+1 \mid k) \tag{7.32}$$

using the Kalman gains

$$K_{k+1} = P(k+1\,|\,k)H^T(t_{k+1})[H(t_{k+1})P(k+1\,|\,k)H^T(t_{k+1}) + \Re_k]^{-1} \tag{7.33}$$

Because the gains are calculated using the history of all past update times and accuracies, the gains automatically increase after missed detections and automatically increase to give greater weight to a detection when it is known to be more accurate, and they automatically decrease as the track ages, reflecting the value of the detections already filtered. For example, for a zero random acceleration, $Q_k = 0$, and a constant detection covariance matrix, $\Re_k$, the $\alpha - \beta$ filter can be made equivalent to the Kalman filter by setting

$$\alpha = \frac{2(2k-1)}{k(k+1)} \tag{7.34}$$

and

$$\beta = \frac{6}{k(k+1)} \tag{7.35}$$

on the kth scan. Thus, as time passes, α and β approach zero, applying heavy filtering to the new samples. In practical radar applications $Q_k > 0$, and so the tracking gains eventually settle to a non-zero value termed the *steady-state tracking gains.*

The tradeoffs for employing a Kalman filter for radar tracking generally are tuning the filter for the desired degree of filtering, selecting the tracking coordinates, and adapting the filter to deal with changes in the target motion (e.g., maneuvers, different phases of ballistic flight, and so on).

Tuning the Kalman Filter. The greatest advantage of the Kalman filter for radar tracking is that it provides a systematic way of calculating gains. However, a disadvantage is that this gain calculation assumes linear target motion with random perturbations (Eq. 7.22). Most practical radar-tracking problems involve targets that deviate from linear motion in more complex ways (e.g., course corrections, terrain following, evasive maneuvers, and atmospheric drag). The Kalman filter is tuned to a practical radar-tracking problem through the selection of the covariance matrix, $Q(t_k)$, of the unknown random maneuver. The goal of this selection is to obtain the best possible tracking performance for the more complex cases of interest while still using the simple Kalman random perturbation model. For example, in the simplified case of a single dimension and constant tracking conditions, the measurement covariance matrix is simply a single, constant measurement variance, $\Re_k = \sigma_m^2$, and the time between detections is a constant $R_k = T$. In this case, the Kalman filter described in Eqs. 7.29 to 7.33 has gains that are a function of the dimensionless track-filtering parameter γ_{track}:

$$\gamma_{\text{track}} = \frac{qT^3}{\sigma_m^2} \tag{7.36}$$

Because the radar measurement accuracy, as represented by the covariance matrix $\Re$, and the time between detection opportunities, T, are parameters of the radar design itself, the selection of $Q(t_k)$ is the degree of freedom available to the tracking filter design. Table 7.4 summarizes the methods for tuning the Kalman filter.

TABLE 7.4 Comparison of Methods of Tuning Kalman Filter for Practical Radar Tracking Problems

Maneuver Model	Q-submatrix	Steady-state Gain Relation and Tracking Index	Tuning Method	Characteristics
Model no. 1: White noise (spectral density q g^2/Hz) acceleration sampled by radar measurement[45].	$q\begin{vmatrix} T_k^3/3 & T_k^2 \\ T_k^2 & T_k \end{vmatrix}$	$\beta = 6 - 3\alpha - \sqrt{3\alpha^2 - 36\alpha + 36}$ and $\gamma_{\text{track}} = \dfrac{qT^3}{\sigma_m^2}$	Vary q to increase/decrease gains and obtain desired performance using equations in Table 7.3.	Accommodates variable measurement rates well. Responds to maneuvers but not at the edge of filter stability.
Model no. 2: Random change in acceleration at each measurement interval. Standard deviation of acceleration change is σ_a.[46,47]	$\sigma_a^2\begin{vmatrix} T_k^4 & T_k^3/2 \\ T_k^3/2 & T_k^2 \end{vmatrix}$	$\beta = 2(2-\alpha) - 4\sqrt{1-\alpha}$ and $\gamma_{\text{track}} = \dfrac{\sigma_a^2 T^4}{\sigma_m^2}$	Vary σ_a to increase/decrease gains and obtain desired performance using equations in Table 7.3.	Responds very well to maneuvers, but operates at the edge of filter stability. Higher radar measurement rate can actually result in less accurate track.[48]
Model no. 3: Random change in velocity at each measurement interval.[49]	$\sigma_v^2\begin{vmatrix} 0 & 0 \\ 0 & 1 \end{vmatrix}$	$\beta = \dfrac{\alpha^2}{(2-\alpha)}$ and $\gamma_{\text{track}} = \dfrac{\sigma_v^2 T^2}{\sigma_m^2}$	Vary σ_v to increase/decrease gains and obtain desired performance using equations in Table 7.3.	Very conservative with respect to filter stability.

TABLE 7.4 Comparison of Methods of Tuning Kalman Filter for Practical Radar Tracking Problems (*Continued*)

Maneuver Model	Q-submatrix	Steady-state Gain Relation and Tracking Index	Tuning Method	Characteristics
Model no. 4: Constantly accelerating target with a white noise jerk j [(g/s)^2/Hz] sampled by radar measurement. (Jerk is the rate of change of acceleration.) [50,51]	$j\begin{vmatrix} \frac{T_k^5}{20} & \frac{T_k^4}{8} & \frac{T_k^3}{6} \\ \frac{T_k^4}{8} & \frac{T_k^3}{3} & \frac{T_k^2}{2} \\ \frac{T_k^3}{6} & \frac{T_k^2}{2} & T_k \end{vmatrix}$	Steady-state gain calculations described in Fitzgerald.[49] and $\gamma_{\text{track}} = \frac{jT^5}{\sigma_m^2}$.	Select this model when target is known/ expected to be accelerating.	Zero lags to constant acceleration; however, noise errors are much greater.[50]
Model no. 5: Constant, deterministic acceleration a (g). Filter objective is to minimize lag plus c standard deviations.[51,52]	Q submatrix not applicable. Instead, assume constant parabolic motion $\frac{1}{2}at^2$.	$\beta = 2(2-\alpha) - 4\sqrt{1-\alpha}$ and $\gamma_{\text{track}} = \frac{a^2T^4}{c^2\sigma_m^2}$.	Vary a to increase/ decrease gains and obtain desired performance using equations in Table 7.3.	Filter minimizes error for a worst-case deterministic maneuver vice a random one.

As seen in Figure 7.28, the selection of $Q(t_k)$ and thus γ_{track} allows one to uniquely determine the steady-state tracking gains as a function of γ_{track}. One can see that large assumed maneuvers (large q, α_a, or a); larger time between updates, T; or very accurate radar measurements (small $\Re$) will result in large tracking gains. The position gain α is nearly identical for the $Q(t_k)$ models no. 1, 2, 3, and 5 in Table 7.4. However, the velocity gain β differs considerably. For random changes in acceleration at each measurement interval (model no. 2), the gains increase to $(\alpha, \beta) = (1,2)$, which is the limit of filter stability. Thus, this model produces filter gains that are the most aggressive at minimizing lags to maneuvers—at the expense of larger

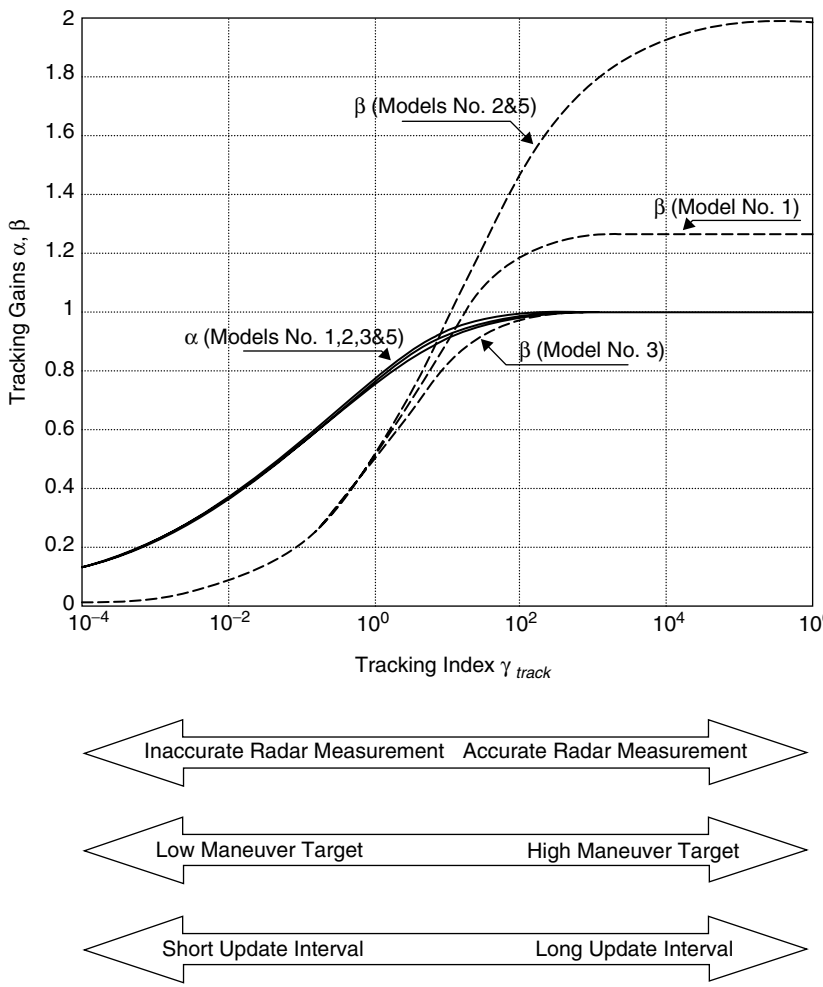

FIGURE 7.28 The relationship between the steady-state tracking gains α and β is shown for different $Q(t_k)$ s corresponding to different assumptions about the unknown target maneuver. Model no. 1: white noise acceleration sampled at each measurement interval; model no. 2: random change in acceleration at each measurement interval; model no. 3: random change in velocity at each measurement interval; and model no. 5: constant deterministic acceleration. Model no. 4 not shown as it is a 3 gain model.

tracking errors due to radar measurement noise. For random changes in velocity at each measurement interval (model no. 3), the gains increase to $(\alpha, \beta) = (1,1)$, which is very conservative from a filter stability point of view. For white noise acceleration sampled by radar measurements (model no. 1), the gains are a compromise, increasing to $(\alpha,\beta) = (1,(3-\sqrt{3}))$. Because this model is a sampled continuous time acceleration, it is preferred when update times are variable because the target does not maneuver more or less when the update interval changes.

The equations in Table 7.3 can then be used to calculate the filter performance in terms of variance reduction ratios and tracking lags. Adjustments to parameters of γ_{track} can be made to obtain the desired noise and lag tradeoff.

Selection of Tracking Coordinates. The Kalman filter assumes linear target motion and a linear relation between the radar detections and the target coordinates. However, radars make detections in polar coordinates (range, angle, doppler), while target motion is most likely linear in Cartesian coordinates (x, y, z). Therefore, some compromises must generally be made in selecting a coordinate system for filtering. Table 7.5 describes the design tradeoffs for different selections.

The polar Kalman filter is rarely used because of the pseudo-accelerations introduced by propagating the state in polar coordinates. The Cartesian/Earth-centered Kalman filter can work well but may have difficulty accommodating radar measurements of less than three dimensions. The extended/dual coordinate system Kalman filter prevents pseudo-accelerations and accommodates measurements of any dimensionality. Both the Cartesian/Earth-centered Kalman filters involve nonlinear transformations resulting in an imperfect calculation of the tracking accuracy. When prediction times are long and/or when very accurate results are needed, these imperfections in the Kalman filter covariance calculation can be significant, and the tracking errors can be quite non-gaussian. Particle filters typically propagate a large number of random samples (particles) from a state transition prior distribution to estimate posterior distributions that are not required to be gaussian in form. Thus, in a particle filter, even multi-modal distributions can be used as prior and realized as posterior distributions. However, particle filters require quite a bit of computation.

The unscented Kalman filter[55] more efficiently calculates the tracking accuracy by propagating selected cardinal points through the filter. The unscented Kalman Filter approximates the covariance matrix with a set of $2L + 1$ sample points, where L is the number of state dimensions. The sample points are propagated through an arbitrary transform function and then used to reconstruct a gaussian covariance matrix. This technique has the advantage of representing the covariance accurately to the third order of a Taylor series expansion. As a result, the calculated tracking accuracy is (at least to third order) uncontaminated (or "unscented") by the nonlinearity.

Adapting Filter to Deal with Changes in Target Motion. The Kalman filter assumes linear target motion perturbed by a random maneuver model as a mathematical convenience in calculating tracking gains. However, most radar targets do not move in a random maneuver but instead move linearly at times and then maneuver unpredictably at times. The challenge in adapting the filter to deal with changes in the target motion (e.g., maneuvers, ballistic re-entry) is to adapt the target motion model for the Kalman filter over time so that more accurate tracking occurs than with a single model. The simplest form of adaptation is a maneuver detector to monitor the tracking filter residuals (differences between measured and predicted position). Large, correlated

TABLE 7.5 Advantages and Disadvantages of Employing the Kalman Filter in Different Coordinate Frames

Kalman Filter Coordinate Frame Variants	Coordinates for Gain Calculation (Eqs. 7.32, 7.33) and state update (Eq. 7.31)	Coordinates for State Prediction (Eqs. 7.29, 7.30)	Method of Covariance Propagation	Advantages	Disadvantages
Polar Kalman filter	Polar	Polar	Eqs. 7.29 to 7.33 in polar coordinates	Filter covariances are calculated exactly and state errors gaussian distributed. Radar detections of less than three dimensions can be used.	Pseudo-accelerations introduced in state propagation.
Cartesian/ Earth-Centered Kalman filter[53]	Cartesian/ Earth-centered	Cartesian/ Earth-centered	Eqs. 7.29 to 7.33 in Cartesian/ Earth-centered coordinates	State propagation is linear (no pseudo-accelerations).	Filter covariances are not exact due to nonlinear transformation.
Extended/ dual coordinate Kalman filter[54]	Polar	Cartesian/ Earth-centered	Eqs. 7.29 to 7.33 in polar coordinates	State propagation is linear (no pseudo-accelerations). Radar detections of less than three dimensions can be easily accommodated.	Requires frequent coordinate transforms.
Unscented Kalman filter[55]	Polar or Cartesian/ Earth-centered	Cartesian/ Earth-centered	Covariance inferred by propagating multiple states	State propagation is linear (no pseudo-accelerations). Filter covariance more exact than traditional methods—particularly for long extrapolation times.	More complex but not necessarily more computation.

residuals generally indicate a maneuver (a deviation from the filter model). Upon maneuver detection, the maneuver spectral density, q, is increased in the Kalman filter model, resulting in higher tracking gains and better following of the maneuver.

A more complex approach is to use multiple Kalman filters running simultaneously with different target motion models—generally, different q values or different equations for target motion (e.g., constant acceleration or constant velocity). Figure 7.29 shows a bank of multiple parallel filters all fed by the same stream of associated measurements. At each detection time, t_k, one of the several filter outputs must be selected to be the track state used for detection to track association.

A systematic way of employing multiple target motion models is the Interacting Multiple Model (IMM) approach diagrammed in Figure 7.30.[56] Multiple models run simultaneously; however, they do not run independently. Instead, there is mixing of

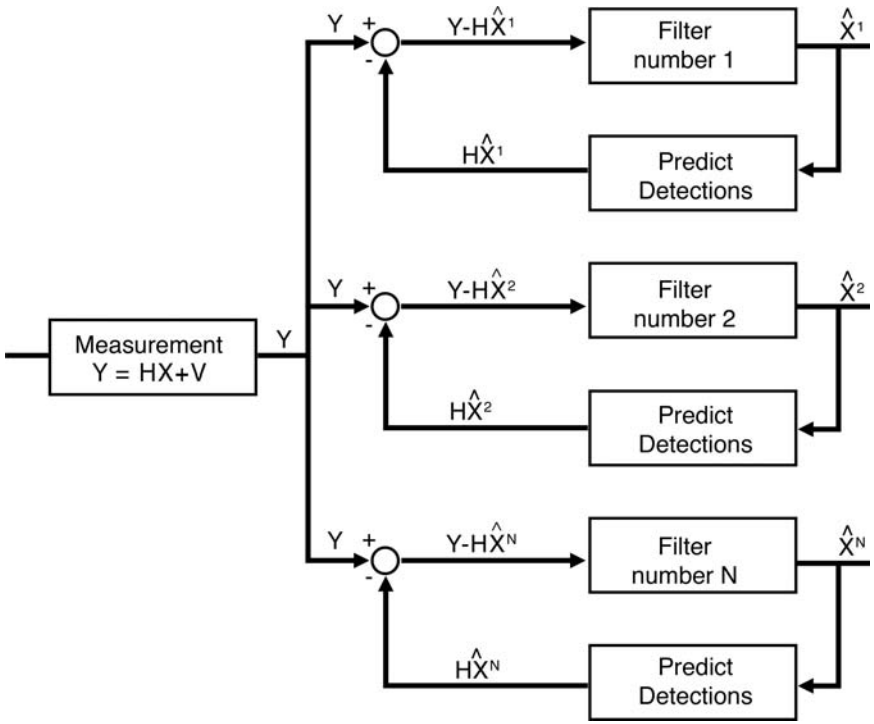

FIGURE 7.29 Bank of parallel radar-tracking filters, each employing a different target motion model (*after S. Blackman and R. Popoli*[44] *© Artech House 1999*)

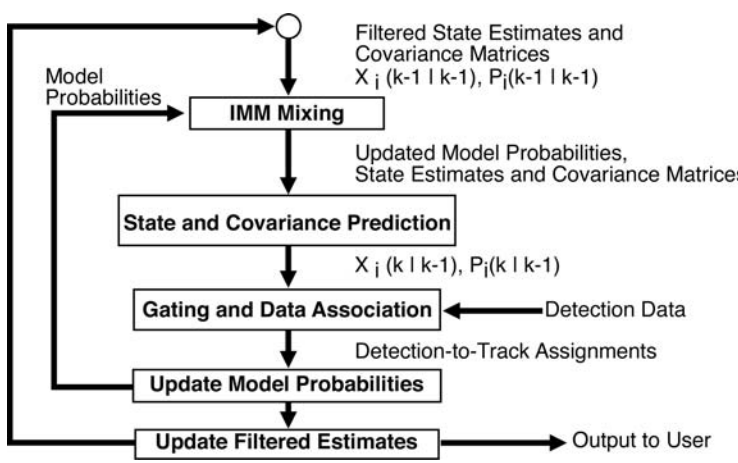

FIGURE 7.30 Flowchart of interacting multiple models (*after S. Blackman and R. Popoli*[44] *© Artech House 1999*)

the model states. The update equation for the *i*th model depends not only on the ith model state but also on the states of all other models. These states are mixed using inferred probabilities of the target transitioning from one motion model to another.

As an example, consider radar tracking of a ballistic missile that undergoes distinct phases of flight: boost, exo-atmospheric flight, and endo-atmospheric re-entry. Each of these phases of flight has a distinct target model.[57] During boost, the target is continually accelerating and increasing speed. This acceleration is unknown and must be estimated. During exo-atmospheric flight, the object is falling with the known acceleration of gravity. During endo-atmospheric re-entry, the target continues to fall but experiences a drag acceleration due to its ballistic coefficient (an unknown target parameter related to the shape and mass of the target). An IMM filter can be used to systematically transition between these different phases of flight, providing a single filter output. Figure 7.31 shows the model probabilities for such an IMM filter application.

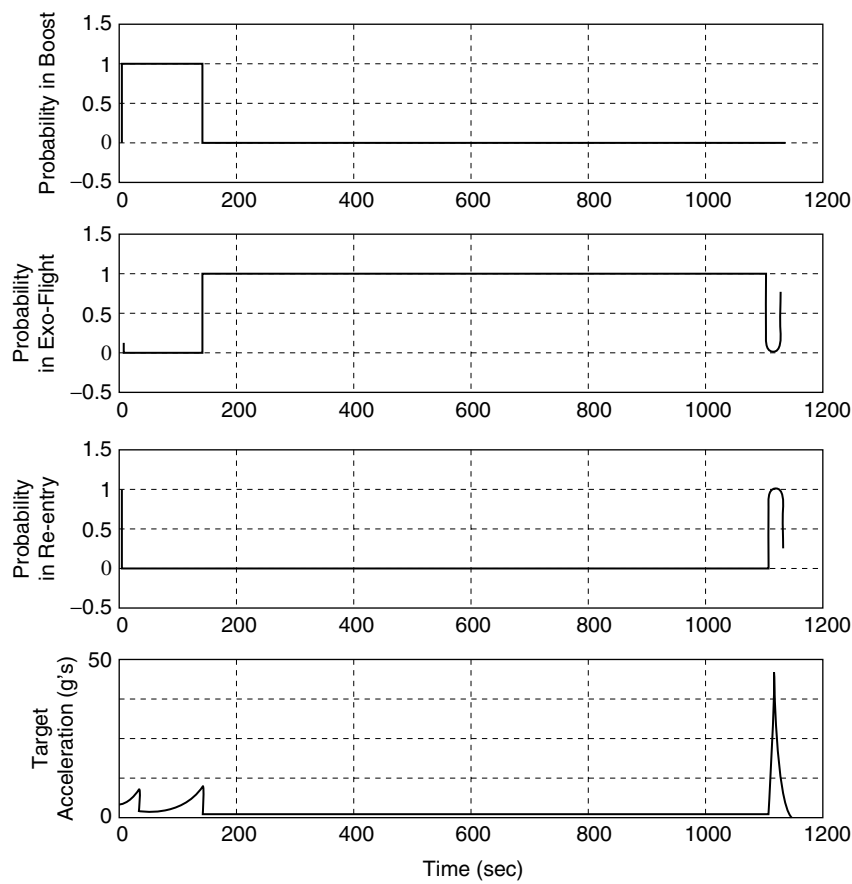

FIGURE 7.31 Model probabilities resulting from the application of an IMM filter to a ballistic missile tracking problem: (*a*) probability that target motion is "boost phase," (*b*) probability that target motion is "exo-atmospheric" flight, (*c*) probability that target motion is "endo-atmospheric" re-entry. (*after R. Coopermanr*[57] *© Fifth International Conference on Information Fusion, vol. 2, 2002*)

Association of Accepted Detection with Existing Tracks. The goal of detection-to-track association is to correctly assign radar detections to existing tracks so the track states in the track file can be correctly updated. The basis for assignment is a measure of how close together the detection and track are in terms of measurable parameters such as range, angle, doppler, and, when available, target signature. The statistical distance is calculated as a weighted combination of the available detection-to-track coordinate differences. In the most general case, this is a complex quadratic form:

$$D^2 = (Y_{k+1} - h(\hat{X}(t_{k+1} \mid t_k))[H(t_{k+1})P(k+1 \mid k)H^T(t_{k+1}) + R_k]^{-1}(Y_{k+1} - h(\hat{X}(t_{k+1} \mid t_k))^T \tag{7.37}$$

For most single radar-tracking problems, it reduces to a simple weighted sum

$$D^2 = \frac{(r_m - r_p)^2}{\sigma_r{}^2 + \sigma_{\text{pr}}^2} + \frac{(\theta_m - \theta_p)^2}{\sigma_\theta{}^2 + \sigma_{p\theta}^2} + \frac{(\varphi_m - \varphi_p)^2}{\sigma_\varphi^2 + \sigma_{p\varphi}^2} + \frac{(D_m - D_p)^2}{\sigma_D^2 + \sigma_{\text{pD}}^2} \tag{7.38}$$

where (r_m, θ_m, φ_m, D_m) are the measured range, azimuth, elevation, and doppler with accuracies (σ_r, σ_θ, σ_φ, σ_D); (r_p, θ_p, φ_p, D_p) are the range, azimuth, elevation, and doppler predicted by the automatic tracker with accuracies (σ_{pr}, $\sigma_{p\theta}$, $\sigma_{p\varphi}$, σ_{pD}). The predicted accuracies are a byproduct of the radar tracking filter. Statistical distance rather than Euclidean distance must be used because the range accuracy is usually much better than the azimuth accuracy.

When targets are widely spaced and in a clear environment, only one target detection pair has a small D^2, making these assignments obvious. Thus, the design of detection-to-track association is usually dominated by the more difficult conditions of closely spaced targets or closely spaced targets and clutter. Figure 7.32 shows a common situation for closely spaced targets and/or clutter. Three association gates are constructed around the predicted positions of three existing tracks. Three detections are made, but assignment of the detections to the tracks is not obvious: two detections are within gate 1; three detections are within gate 2; and one detection is within gate 3. Table 7.6 lists all detections

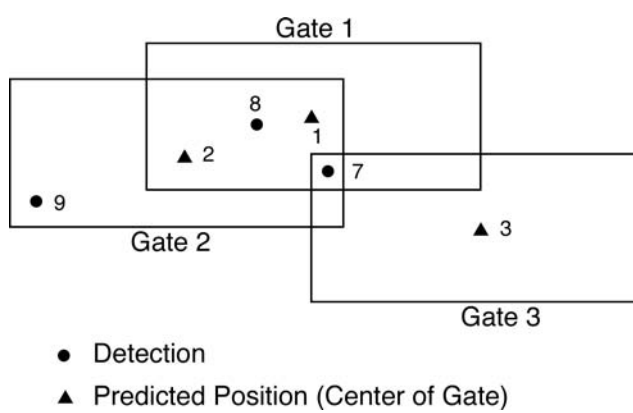

FIGURE 7.32 Examples of the problems caused by multiple detections and tracks in close vicinity (*from G. V. Trunk*[7])

TABLE 7.6 Association Table for Example Shown in Figure 7.32*

Track No.	Detection No. 7	Detection No. 8	Detection No. 9
1	4.2	1.2	∞
2	5.4	3.1	7.2
3	6.3	∞	∞

*(*from G. V. Trunk*[7])

within the tracking gates and the statistical distance between the detection and track. If the detection is outside the track gate, the statistical distance is set to infinity.

Nearest-neighbor assignment is the most common solution to this problem. The simplest form of nearest neighbor works sequentially on incoming data. As each new detection is made, it is assigned to the track with which it has the smallest statistical distance. Hence, if detection no. 9 was received first, it would be assigned to track no. 2. However, it is better to delay the association process slightly so that all detections in a local neighborhood are received and stored and an association table, such as Table 7.6, generated. (This has implications about how sectors are scanned with a phased array.)

Nearest-neighbor assignment can now be applied to the association table by finding the smallest statistical distance between a detection and a track, making that association, and eliminating that detection and track (row and column) from the table. This process is repeated until there are either no tracks or no detections left. Applying this algorithm to Table 7.6 results in detection no. 8 updating track no. 1, detection no. 7 updating track no. 2, and track no. 3 not being updated. Better assignments are possible with more sophisticated processing algorithms. The three types of more sophisticated algorithms most frequently used are

1. *Global Nearest Neighbor (GNN)* Consider the whole matrix of statistical distances simultaneously, and minimize a metric such as the sum of all statistical distances for a complete assignment solution. Performing this optimization can be done using Munkres algorithm.[58] Munkres algorithm is an exact solution of the minimization problem but is rarely used because it is computationally slow. A more computationally efficient exact solution is the Jonker, Volgenant, Castanon (JVC) algorithm.[59] The JVC is much more efficient for sparse assignment matrices (which are likely for practical radar-tracking problems). Speed improvements of 30 to 1000 times have been reported. An effective suboptimal solution is the Auction algorithm, which views the tracks as being "auctioned off" to the detections—iteratively assigning higher costs to tracks competed for by more detections.[60] Figure 7.33 provides a comparison[61] of the Munkres, JVC, and Auction algorithms optimized for sparse data. The JVC and Auction algorithms provide a significant increase in computational speed. Although the Auction algorithm is simpler, requiring less lines of code, the JVC algorithm generally requires less computation time.
2. *Probabilistic Data Association (PDA)* Another alternative is the probabilistic data association (PDA) algorithm[62,63,64] where no attempt is made to assign tracks to detections, but instead, tracks are updated with all the nearby detections—weighted by the perceived probability of the track being the correct association. Because PDA relies on erroneous associations essentially "averaging out," it is most effective when tracks are far enough apart that nearby detections originate from spatially random noise or clutter exclusively and when the tracking gains are small (i.e., when the tracking index γ_{track} is small). The Joint Probabilistic Data

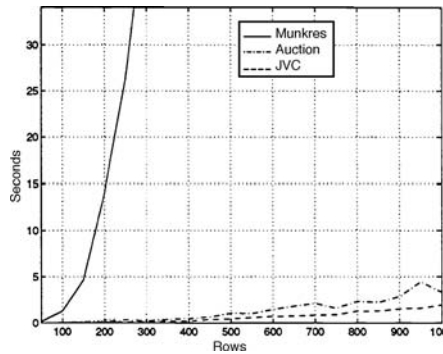

FIGURE 7.33 A comparison of the execution time for the Munkres (optimum), JVC (optimum), and Auction (suboptimum) algorithms shows the rapid increase in computation required for Munkres as the number of rows in the assignment matrix increases. The JVC and auction algorithms show much more gradual growth. (*after I Kadar et al.*[61] *© SPIE.1997*)

Association (JPDA)[65] is an extension of PDA that handles more closely spaced targets. In JPDA, detections are weighted less when they are near another track.

3. *Multiple Hypothesis Algorithms* The most sophisticated algorithms are multiple hypothesis algorithms in which all (or many) possible tracks are formed and updated with each possible detection.[66,67,68] In Table 7.6, track no. 1 would become three tracks (or hypotheses), corresponding to updating with detection no. 8, detection no. 7, and no detection. Each of these tracks would undergo a Kalman filter update and be eligible for association with the next set of detections. Tracks are pruned away in a systematic manner leaving only the most probable. Figure 7.34 illustrates the tracking of a single target using multiple hypothesis techniques. In this example, many hypotheses are formed and, over successive measurement intervals, successfully pruned away leaving only one correct track.

The region of applicability for the more sophisticated algorithms is determined by two parameters: the density of extraneous detections λ (detections per unit area or volume)

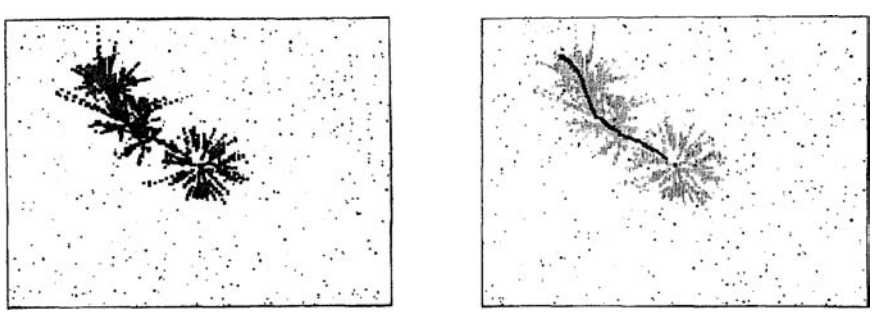

FIGURE 7.34 Example of the use of multiple hypothesis tracking on 90 scans of simulated radar data containing a single target and many false alarms: (*a*) shows all hypotheses forms and (*b*) shows the single hypothesis selected. (Pruned hypotheses are grayed out.) (*after W. Koch*[69] *© IEEE 1995*)

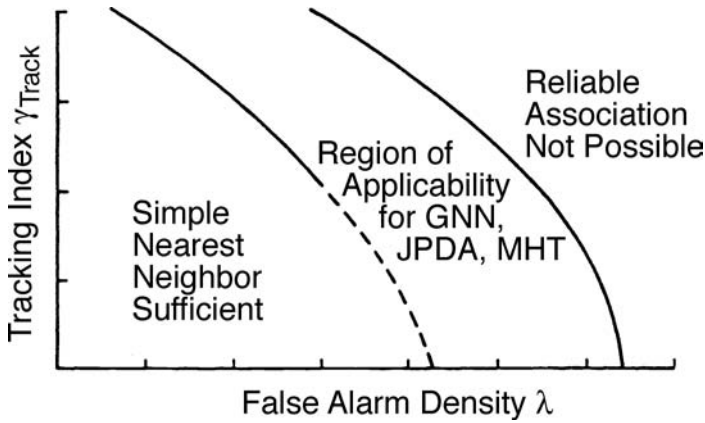

FIGURE 7.35 The applicability of different detection-to-track association algorithms is determined by the density of false alarms and the dimensionless tracking parameter γ_{track}. (*after D. J. Salmond*[70] *© SPIE 1990*)

and the dimensionless track filtering parameter γ_{track}. Figure 7.35 bounds this region of applicability. When λ and γ_{track} are small, then there is no need for any more than simple nearest neighbor tracking, and indeed, most tracking systems still use this approach. As λ increases, there is greater risk of false association decisions; however, the effect of this is reduced if γ_{track} is small. At the other extreme, when λ and γ_{track} are large, the tracking problem is essentially unsolvable without basic changes to the radar design parameters to reduce them. There is an intermediate region where sophisticated association has value. The width of this region is very specific to the particular problem. When γ_{track} is large and very little delay in the output can be tolerated, then the region of applicability is fairly small and very simple multiple hypothesis approaches (splitting tracks into at most one or two hypotheses) are then the best answer.

When γ_{track} is small, then PDA/JPDA can be used to operate at significantly higher false alarm densities. When significant delay can be tolerated in the output, then many hypotheses can be formed (as in Figure 7.34) and orders of magnitude more detections handled. Blackman and Popoli[44] provide a good survey of comparative studies in this area. One study using data recorded from flights of closely spaced aircraft showed very little difference between GNN, JPDA, and MHT.[38] However, theoretical predictions can show differences of orders of magnitude in the density of clutter detections that can be handled.[44]

New Track Formation. There are two classes of track formation algorithms:

1. *Forward-tracking algorithms* basically propagate one hypothesis forward in time, recursively checking for "target-like" motion. Detections that do not correlate with clutter points or tracks are used to initiate new tracks. If the detection does not contain doppler information, the new detection is usually used as the predicted position (in some military systems, one assumes a radially inbound velocity), and a large correlation region must be used for the next observation. The correlation region must be large enough to capture the next detection of the target, assuming that it could have the maximum velocity of interest. A common track initiation

criterion is four out of five, although one may require only three detections out of five opportunities in regions with a low false-alarm rate and a low target density. However, one may require a much larger number of detections when the radar has the flexibility of an electronic scan that can place many detection opportunities in a short time interval.

2. *Backward-tracking or "batch" algorithms* consider all the detections simultaneously, attempting to match the detections to a "target-like" pattern. This can be done by actually constructing a large number of matched filters, as in retrospective processing[71] (see Figure 7.36), or by using a forward-tracking process with multiple hypothesis formed and propagated.

Just as automatic radar detection is a tradeoff between probability of detection and probability of false alarm, new track formation is a tradeoff between the speed at which a track is formed and the probability of erroneously forming a false track that does not represent a physical object of interest. There are two types of false tracks: (1) Tracks on real objects that are simply not of interest. For example, if the targets of interest are airplanes, then a false track could be a track on a bird. (2) Tracks composed of unrelated detections from different objects that the automatic tracking process has mistakenly associated together. For example, a false track could be composed of detections from several different stationary clutter points that have been associated together over time to create a false moving track.

The approach for preventing false tracks on objects not of interest is to actually develop tracks on all of them but then observe them long enough to classify them as unwanted. In the case of the bird, one would gather enough detections to improve the velocity accuracy of the track so that it is clear whether the track is of interest or not. Thus, one desires to delay the disclosure of a track until enough time has passed to classify it accurately. This accuracy can be determined by T_{obs}, the amount of time over which the object is observed and by basic parameters of the radar:

T = the time between successive detections

σ = the accuracy in a particular dimension of interest

M = the number of detections used in forming the track

$N \cong (T_{\text{obs}}/T) + 1$, which is the number of detection opportunities

The velocity accuracy is given by the following equation:[72]

$$\sigma_v = \frac{\sigma}{T_{\text{obs}}} \times \left[\frac{12(N-1)}{N(N+1)}\right]^{1/2} \tag{7.39}$$

The dominant design parameters in the equation are the accuracy of the radar and the observation time. (Better accuracy or longer observation time allows more accurate measurement of velocity.) Making more detections in the observation time improves the accuracy but only in a square-root sense.

The approach to preventing falsely composed tracks from different objects in a clutter region, G, is to require enough detections in a tight enough pattern to make $E[N_{\text{FT}}]$, the expected number of false tracks, small. When there is an average of N_C detections in a D-dimensional region G, then[73]

$$E[N_{\text{FT}}] = \lambda_F \times \lambda_p^{M-2} \times N_C^M \times \gamma(D, N, M) \tag{7.40}$$

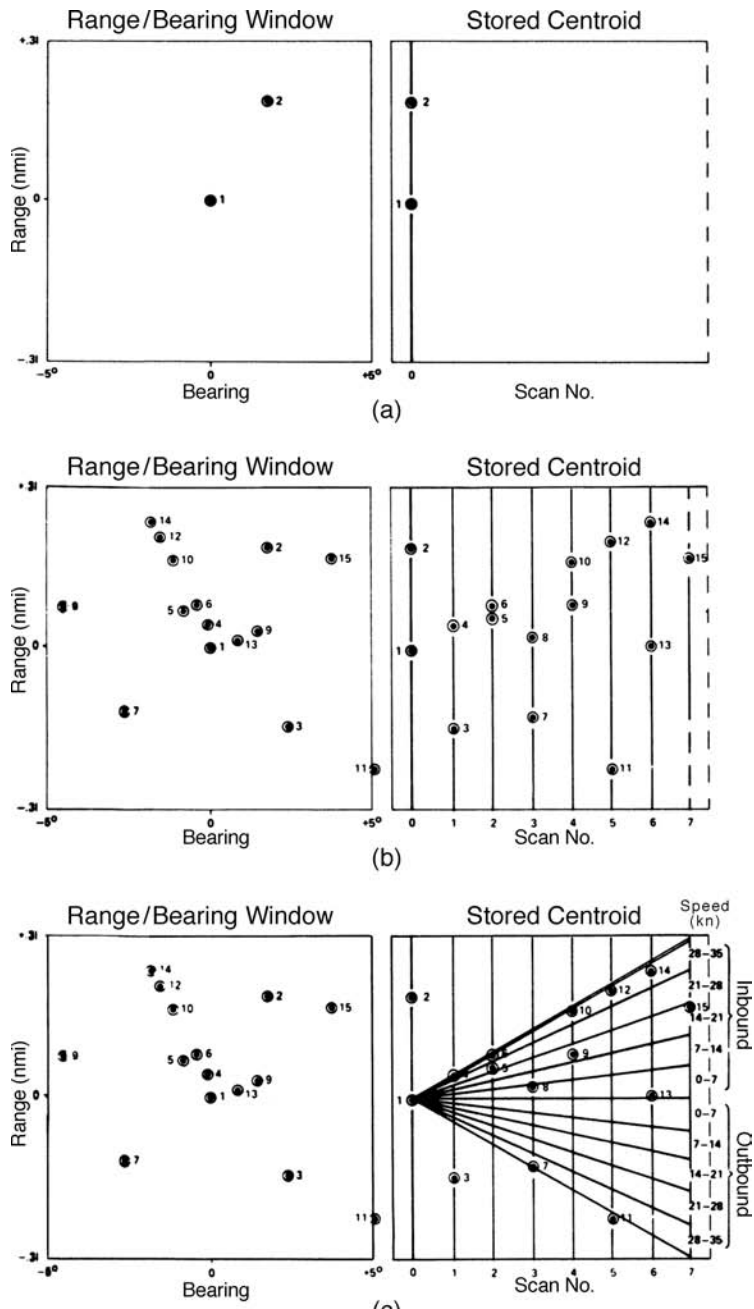

FIGURE 7.36 The retrospective process: (*a*) a single scan of data, (*b*) eight scans of data, and (*c*) eight scans of data with trajectory filters applied (*after Prengaman et al.*[71] © *IEEE 1982*)

where λ_F is the ratio of the size of the possible space a target can travel in one detection interval to the size of entire clutter region G,

$$\lambda_F = \frac{(V_{\text{MAX}})^D}{G} \tag{7.41}$$

and λ_P is the ratio of the size of a radar resolution cell to the size of the entire clutter region G

$$\lambda_P = \frac{\tau_1 \cdot \cdot \cdot \tau_D}{G} \tag{7.42}$$

τ_i being the resolution "distance" in the ith dimension, and $\gamma(D, N, M)$ being the combinatorial term:

$$\gamma(D,N,M) = (N-1)^D \binom{N-1}{M-1} 2^{D(M-1)} \tag{7.43}$$

Figure 7.37 gives an example of the application of Eqs. 7.40 to 7.43 to a radar with $\lambda_P = 2.10^{-3}$ and $\lambda_P = 10^{-5}$. Increasing the number of detections required to form

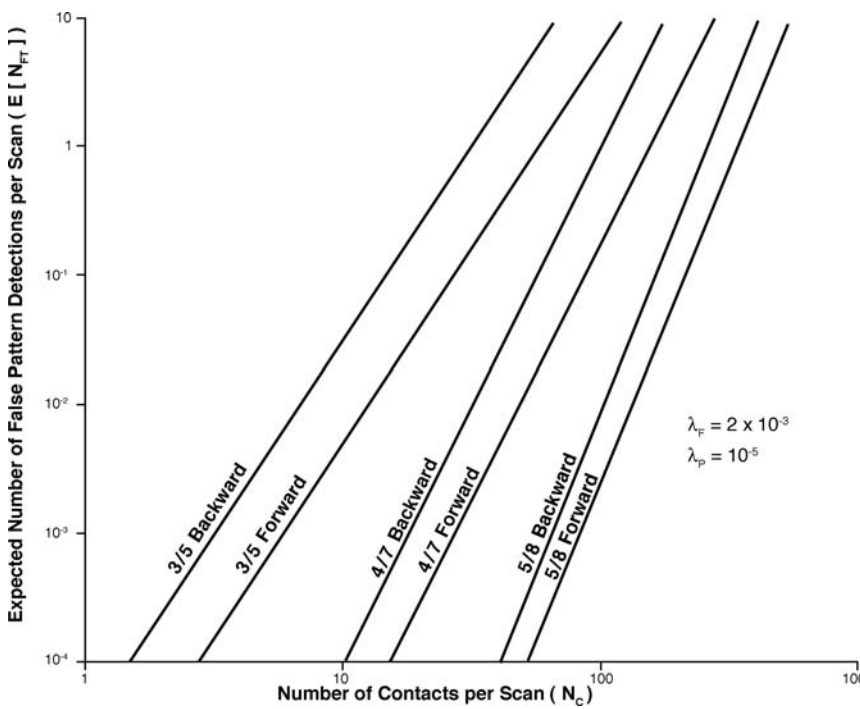

FIGURE 7.37 Variation of the expected number of false tracks with the track formation M-out-of-N criterion (*after W. G. Bath et al.*[73])

a track from three (out of five) to five (out of eight) increases the density of false alarms that can be tolerated by more than an order of magnitude. Forward- and backward-tracking algorithms produce similar numbers of false tracks. However, the backward-tracking algorithms can operate in more ambiguous situations (where the density of false alarms, λ, is comparable to or greater than λ_F or λ_P). Under these ambiguous circumstances, the forward tracker will have multiple detections in a track formation or promotion gate and will require multiple hypothesis to reliably form tracks.

The design of the track formation process and the automatic detection process should be considered together. A longer time allowed for track formation (higher *M*/*N*) allows the radar detection process to use lower detection thresholds, resulting in better radar sensitivity. For any given set of radar parameters, *M*/*N* track formation criterion, and probability distribution of clutter amplitudes, there exists an optimum false-alarm rate that minimizes the signal-to-noise ratio required to detect targets. Figure 7.38 illustrates this optimization for an eight-scan track formation process.

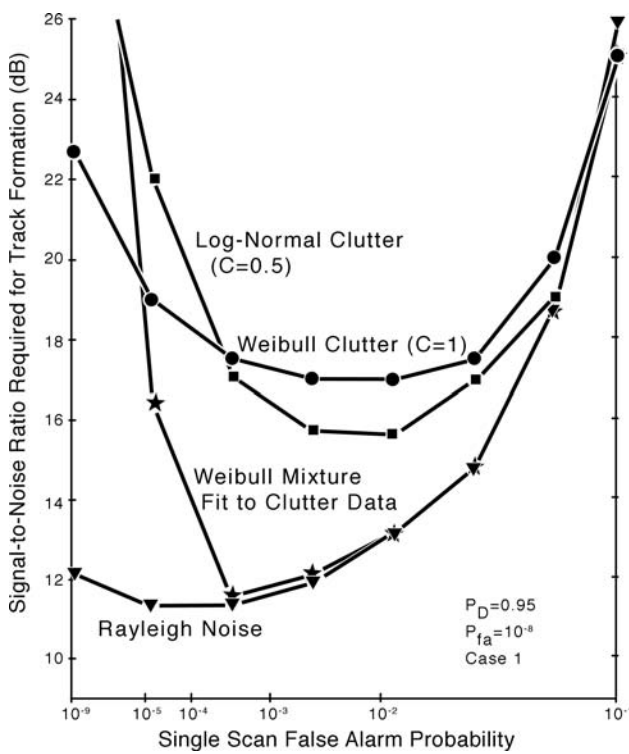

FIGURE 7.38 Overall sensitivity of an automatic detection and automatic tracking process working together. The single-scan false-alarm probability can be optimized to provide the lowest required signal-to-noise ratio for various probability distributions of clutter amplitude. (*after Prengaman et al.*[74] © *IEEE 1982*)

Very low single-scan false-alarm probabilities allow tracks to be formed quickly. However, if a longer delay is tolerable, then detection thresholds can be lower, resulting in better sensitivity in non-gaussian clutter.

Radar Scheduling and Control. The interaction of the radar-tracking system with the scheduling and control function of the radar is minor for mechanical rotating radars but major for phased array radars. For mechanically rotating radars, all that is usually done is that the tracking gates are fed back to the signal processor. The tracking gates are always used to facilitate the association process and may be used to lower the detection threshold within the gate and/or modify the contact entry logic within the gate (e.g., modify rules governing clutter maps).

The interaction of the tracking system with a phased array radar is much more significant. The major benefit of a phased array with respect to tracking is in the area of track initiation.[75,76] Phased arrays use a confirmation strategy to initiate tracks rapidly. That is, after the association process, all unassociated detections generate confirmation dwells to confirm the existence of a new track. The initial confirmation dwell uses the same waveform (frequency and PRF, if a pulse-doppler waveform) but may increase the energy. Analysis has shown that a 3-dB increase in the transmitted confirmation energy (additional energy is also available by placing the target in the center of the confirmation beam) can significantly increase the probability of confirmation.[76] Furthermore, the confirmation dwell should be transmitted as soon as possible to maintain a Swerling I fluctuation model. (That is, if the target was originally detected when the target fluctuation produced a large return, the confirmation dwell will see this same large return.) After confirmation, a series of initial track maintenance dwells over several seconds is used to develop an accurate state vector. A complete discussion of priority associated with tracking within the scheduler of a phased array is beyond the scope of this brief discussion. However, it is worthwhile noting these general rules: (1) Confirmation dwells should have a priority higher than all other functions except those associated with weapon control; (2) low priority tracks (e.g., tracks at long range) can be updated using search detections; and (3) high priority tracks should have a priority higher than volume surveillance. The update rate for high priority tracks should be such that a single tracking dwell is sufficient to update the track. The actual update rate will depend on many factors including (a) maximum target speed and maneuver capability, (b) radar beamwidth (beam could be spoiled), (c) range of the radar track, and (d) accuracy of predicted position. If a pulse doppler dwell is required to update the track in clutter, the waveform should be selected to place the target near the center of the ambiguous range-doppler detection space. Finally, the track can be updated with the ambiguous range-doppler detection because the track state-vector can be used to remove the ambiguity.

7.4 NETWORKED RADARS

Ideally, a single radar can reliably detect and track all targets of interest. However, the environment and the laws of physics often will not permit this. In general, no single radar can provide a complete surveillance and tracking picture. Radar networking can be a good solution to this problem and, in some cases, may be more cost effective than solving the problem through one very high performance radar. Radar networking systems are generally characterized by what radar data are shared and how they are correlated and fused. The two most common ways of combining radar data are as follows:

1. Detection-to-track fusion (see Figure 7.39, upper half) associates each detection to the networked track, calculated potentially using detections from all radars. Thus, the entire stream of detections (up to the present) is potentially available to calculate the track state used for the association decision on the most recent detection.
2. Track-to-track fusion (see Figure 7.39, lower half) associates each detection to a single radar track state calculated using only detections from that radar. The single radar track states are then grouped with each other to produce a netted track state.

The design decision as to which approach is better for grouping data depends on the radars and targets involved. One case where detection-to-track association is clearly better is when the radars have a reduced probability of detection so there are potential gaps in the data stream or periods where the data stream is sparse. In these cases, a much more accurate track state can be calculated using multiple data streams than using only one because multiple streams will tend to fill in the gaps in detection and restore a high consistent data rate during periods of reduced probability of detection. Figure 7.40 illustrates the sensitivity to target fades by plotting the track region of uncertainty (ROU) versus the probability of detection for single radar tracking and multiple radar tracking. The ROU is defined as the distance that contains the error with 99 percent probability and is

$$\text{ROU} = 2.3(\textit{tracking error due to detection noise}) + (\textit{tracking error due to maneuver})$$

This can be calculated for any case of interest using the formulas in Table 7.3.

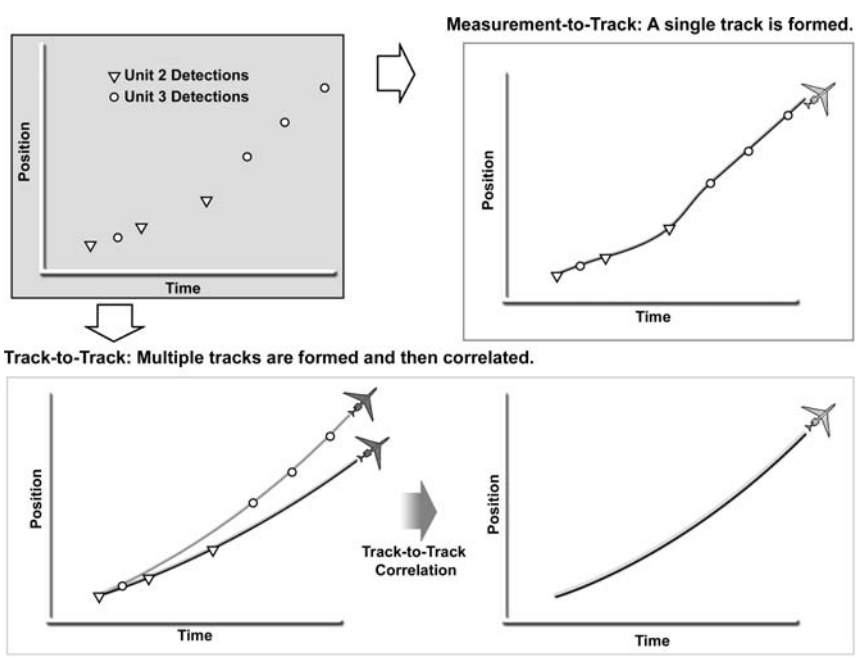

FIGURE 7.39 There are two common methods of fusion data in radar networking: detection-to-track and track-to-track. (*after W. Bath*[77] *© IEE 2002*)

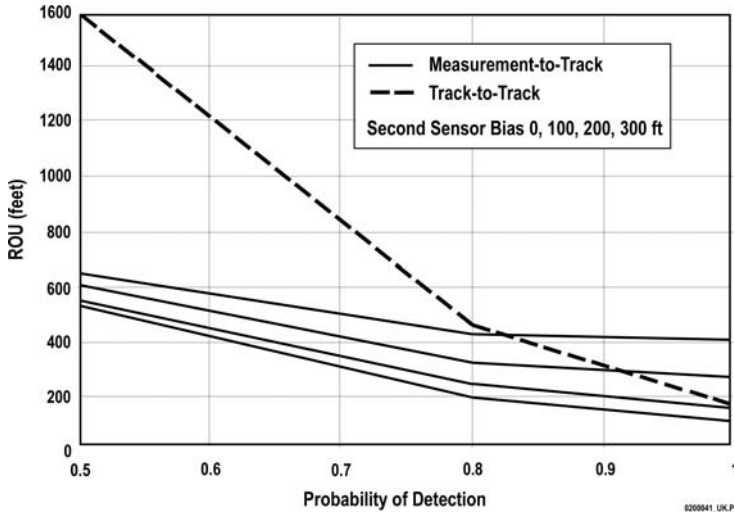

FIGURE 7.40 Comparison of detection-to-track and track-to-track association. For fading targets ($Pd < 1$), detection-to-track is preferred. For large sensor biases and non-fading targets, track-to-track is preferred. (*after W.Bath*[77] © *IEE 2002*)

When the probability of detection is much less than unity, the measurement-to-track fusion is considerably more accurate. This is easily explained by the fact that the probability of a significant outage of data is much reduced if two sources are available. With a more accurate track, tighter association criteria can be used for detections.

If the biases cannot be effectively removed, then there may be an advantage to associating to a single radar track—which by definition is unbiased with respect to itself. If biases cannot be kept smaller than the ROU, then at high probabilities of detection, one prefers single radar association followed by track-to-track association.

It is possible to make simple comparisons between the accuracy of detection fusion as opposed to track fusion for equivalent use of data bandwidth to exchange radar data. When ROU is plotted as a function of the position gain α, it has the "bathtub" shape shown by the single radar curve in Figure 7.41. The left-hand side of the "bathtub" is dominated by the lag component, while the right-hand side is dominated by the radar measurement noise component. Because the gains (horizontal axis) are the designer's choice, the single radar ROU is the minimum of the "bathtub" curve.

Now consider the fusion of two radars in a particular dimension. If one radar has one-tenth the ROU of the other in this dimension, then the more accurate radar in this dimension will dominate and essentially determine the result. At least in steady state, it is relatively easy to produce this dominance by any of the fusion methods. Of more interest is the case where the radars are comparable in terms of accuracy and update rate, producing comparable ROUs. This case more clearly shows the difference in the fusion methods.

For example, when two identical radars are combined by detection fusion, then the update rate is essentially doubled. This reduces the lag by a factor of 4, allowing a smaller gain to be selected (optimization more to the left of the "bathtub"), reducing the tracking errors due to measurement noise. The net result is the movement from the single radar curve to the detection fusion curve in Figure 7.41.

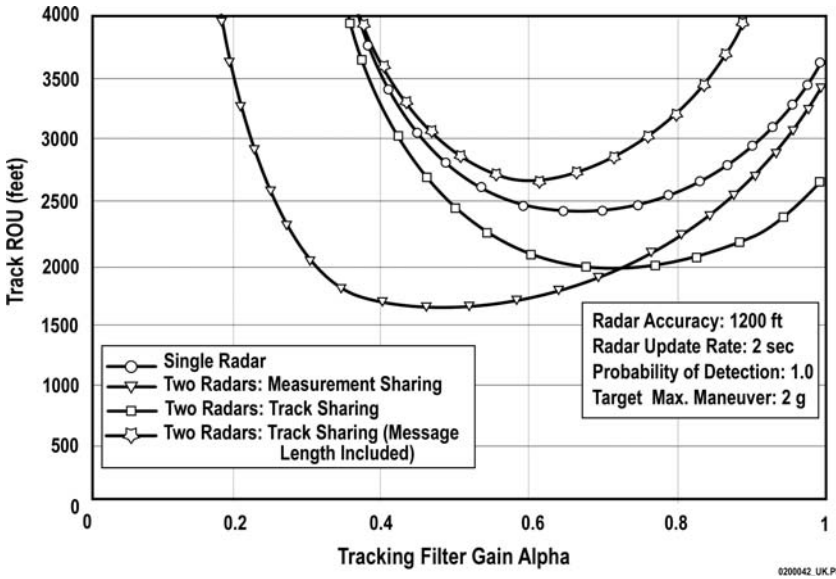

FIGURE 7.41 Comparison of detection fusion and track fusion approaches. For air-breathing targets, detection fusion produces the most accurate track (smallest ROU). (*after W.Bath*[77] *© IEE 2002*)

When two identical radars are combined by track fusion, the update rate for each tracking process does not change, and so the lag does not change. However, the standard deviation of the tracking errors due to measurement noise is reduced by the square root of 2, allowing a larger gain to be selected (optimization more to the right of the bathtub), reducing the lag. The net result is the movement from the single radar curve to the track fusion curve in Figure 7.41.

If there is any significant maneuver possible, the factor of 4 in lag will have a more significant effect than the factor of the square root of 2 in the square root of the tracking errors due to measurement noise. Thus, one can see the detection fusion curve achieves a significantly lower minimum than the track fusion curve.

To combine data from multiple radars, the data must be placed in a common coordinate system. This process is called *grid locking* and involves specifying the location of the radars and estimating radar biases in range and angle. The previous difficult problem of radar location is solved trivially by the global positioning system. An estimate of radar biases between two radars can be obtained from a long-term average of the difference between predicted and measured coordinates on all tracks that have a substantial number of detections from both radars.[78]

7.5 UNLIKE-SENSOR INTEGRATION

A number of sensors can be integrated: radar, identification friend or foe (IFF), the air traffic control radar beacon system (ATCRBS), infrared, optical, and acoustic. The sensors that are most easily integrated are the electromagnetic sensors, i.e., radar, IFF, and strobe extractors of noise sources or emitters.

IFF Integration. The problem of integrating radar and military IFF data is less difficult than that of integrating two radars. The question of whether detections or tracks should be integrated is a function of the application. In a military situation, by integrating detections one could interrogate the target only a few times, identify it, and then associate it with a radar track. From then on, there would be little need for re-interrogating the target. However, in an air traffic control situation using ATCRBS, targets would be interrogated at every scan and, consequently, either detections or tracks could be integrated.

Radar–DF Bearing Strobe Integration. Correlating radar tracks with DF (direction finding) bearing strobes on emitters has been considered by Coleman[79] and later by Trunk and Wilson.[80,81] Trunk and Wilson considered the problem of associating each DF track with either no radar track or one of m radar tracks. In their formulation, there were K DF angle tracks, each specified by a different number of DF detections; and similarly, m radar tracks, each specified by a different number of radar detections. Because each target can carry multiple emitters (i.e., multiple DF tracks can be associated with each radar track), each DF track association can be considered by itself, resulting in K disjoint association problems. Consequently, an equivalent problem is given a DF track specified by n DF bearing detections, one can associate the DF track with no radar track or with one of m radar tracks, the jth radar track being specified by m_j radar detections. Using a combination of Bayes and Neyman-Pearson procedures and assuming that the DF detection errors are usually independent and gaussian-distributed with zero mean and constant variance σ^2 but with occasional outliers (i.e., large errors not described by the gaussian density), Trunk and Wilson argued that the decision should be based on the probability

$$P_j = \text{probability}\ (Z \geq d_j) \tag{7.44}$$

where Z has a chi-square density with n_j degrees of freedom and d_j is given by

$$d_j = \sum_{i=1}^{n_j} \min\{4, [\theta_e(t_i) - \theta_j(t_i)]^2 / \sigma^2\} \qquad j = 1, \ldots, m \tag{7.45}$$

where n_j is the number of DF detections overlapping the time interval for which the jth radar track exists; $\theta_e(t_i)$ is the DF detection at time t_i; $\theta_j(t_i)$ is the predicted azimuth of radar track j for time t_i; and the factor 4 limits the square error to $4\sigma^2$ to account for DF outliers. By using the two largest P_js, designated Pmax and Pnext, and thresholds T_L, T_H, T_M, and R, the following decisions and decision rules were generated:

1. **Firm correlation** DF signal goes with radar track having largest P_j (i.e., Pmax) when $P\text{max} \geq T_H$ and $P\text{max} \geq P\text{next} + R$.
2. **Tentative correlation** DF signal probably goes with radar track having largest P_j (i.e., Pmax) when $T_H > P\text{max} \geq T_M$ and $P\text{max} \geq P\text{next} + R$.
3. **Tentative correlation with some track** DF signal probably goes with some radar track (but cannot determine which) when $P\text{max} \geq T_M$ but $P\text{max} < P\text{next} + R$.
4. **Tentatively uncorrelated** DF signal probably does not go with any radar track when $T_M > P\text{max} > T_L$.
5. **Firmly uncorrelated** DF signal does not go with any radar track when $T_L \geq P\text{max}$.

The lower threshold T_L determines the probability that the correct radar track (i.e., the one associated with the DF signal) will be incorrectly rejected from further consideration. If the desired rejection rate for the correct track is P_R, one can obtain this by setting $T_L = P_R$. The threshold T_H is set equal to P_{fa}, defined as the probability of falsely associating a radar track with a DF signal when the DF signal does not belong with the radar track. The threshold T_H is a function of the azimuth difference μ between the true (DF) position and the radar track under consideration. The threshold T_H was found for $\mu = 1.0\sigma$ and $\mu = 1.5\sigma$ by simulation techniques, and the results for $P_{fa} = 0.01$ are shown in Figure 7.42. Between the high and low thresholds, there is a tentative region. The middle threshold divides the "tentative" region into a tentatively correlated region and a tentatively uncorrelated region. The rationale in setting the threshold is to set the two associated error probabilities equal for a particular separation. The threshold T_M was found by using simulation techniques and is also shown in Figure 7.42.

The probability margin R ensures the selection of the proper DF radar association (avoiding rapidly changing decisions) when there are two or more radar tracks close to one another. The correct selection is reached by postponing a decision until the two highest association probabilities differ by R. The value for R is found by specifying a probability of an association error P_e according to $P_e = P(P\text{max} \geq P\text{next} + R)$, where Pmax corresponds to an incorrect association and Pnext corresponds to the correct association. The probability margin R is a function of P_e and the separation μ of the radar tracks. The probability margin R was found for $\mu = 0.25\sigma$, 0.50σ, and 1.00σ by using simulation techniques, and the results for $P_e = 0.01$ are shown in Figure 7.43.

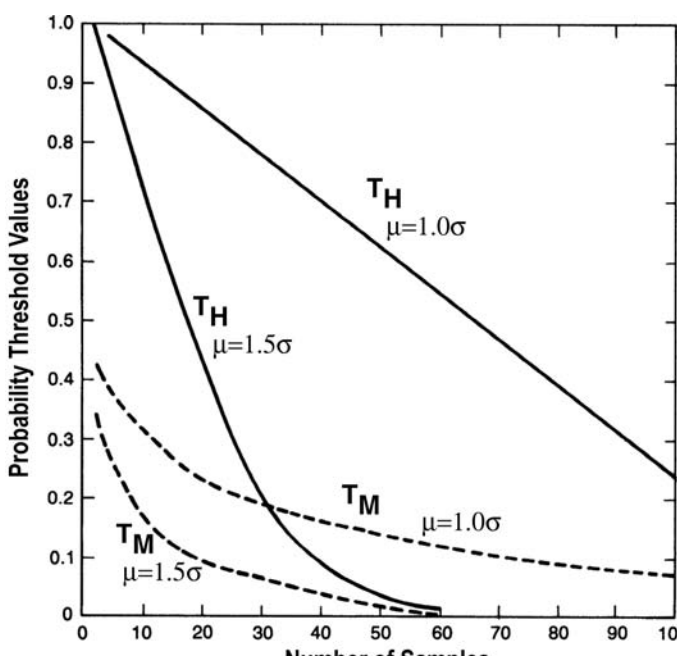

FIGURE 7.42 High threshold (solid lines) and middle threshold (dashed lines) versus number of samples for two different separations (*after G.V. Trunk and J.D. Wilson*[80] *© IEEE 1987*)

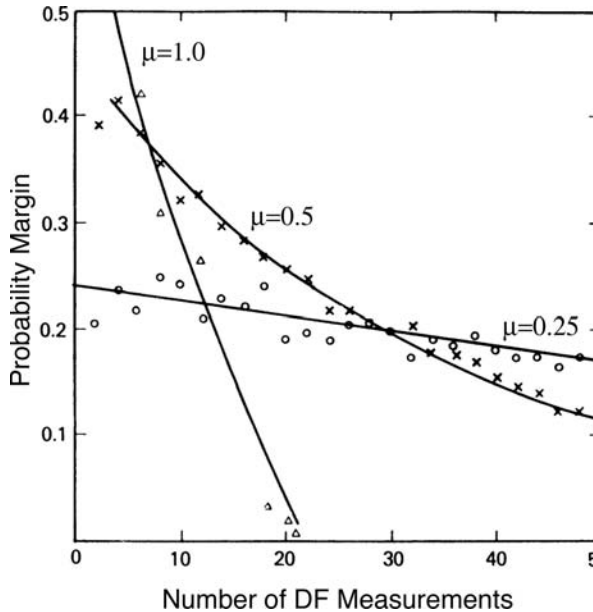

FIGURE 7.43 Probability margin versus number of DF detections for three different target separations. The *o*s, *x*s, and Δs are the simulation results for $\mu = 0.25$, $\mu = 0.5$, and $\mu = 1.0$, respectively. (*after G.V. Trunk and J.D. Wilson*[80] *© IEEE 1987*)

Because the curves cross one another, one can ensure that $P_e \leq 0.01$ for any μ by setting R equal to the maximum value of any curve for each value of n.

The algorithm was evaluated by using simulations and recorded data. When the radar tracks are separated by several standard deviations of the detection error, correct decisions are made rapidly. However, if the radar tracks are close to one another, errors are avoided by postponing the decision until sufficient data are accumulated. An interesting example with recorded data is shown in Figures 7.44 and 7.45. Figure 7.44 shows the radar (azimuth) detections of the control aircraft, the radar detections of four aircraft of opportunity in the vicinity of the control aircraft, and the DF detections on the radar on the control aircraft. The association probabilities, with and without limiting in Eq. 7.45, are shown in Figure 7.45. Initially, an aircraft of opportunity has the highest association probability; however, a firm decision is not made because *P*max does not exceed *P*next by the probability margin. After the 14th DF detection, the emitter is firmly correlated with the control aircraft. However, at the 18th DF detection, a very bad detection (outlier) is made, and the firm correlation is downgraded to a tentative correlation if limiting is not used. If limiting is employed, however, the correct decision remains firm.

In a complex environment where there are many radar tracks and DF signal sources, it is quite possible that many DF signals will be assigned the category that the DF signal probably goes with some radar track. To remove many of these ambiguities, multisite DF operation can be considered. The extension of the previous procedures

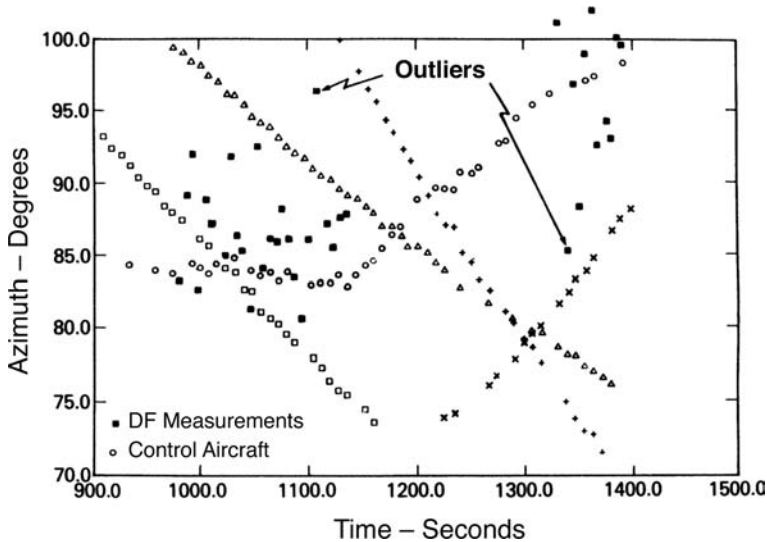

FIGURE 7.44 Radar detections *o* and DF detections collected on the control aircraft. The *o*s, Δs, +s, and *x*s are radar detections on four aircraft of opportunity in the vicinity of the control aircraft. (*after G.V. Trunk and J.D. Wilson*[80] *© IEEE 1987*)

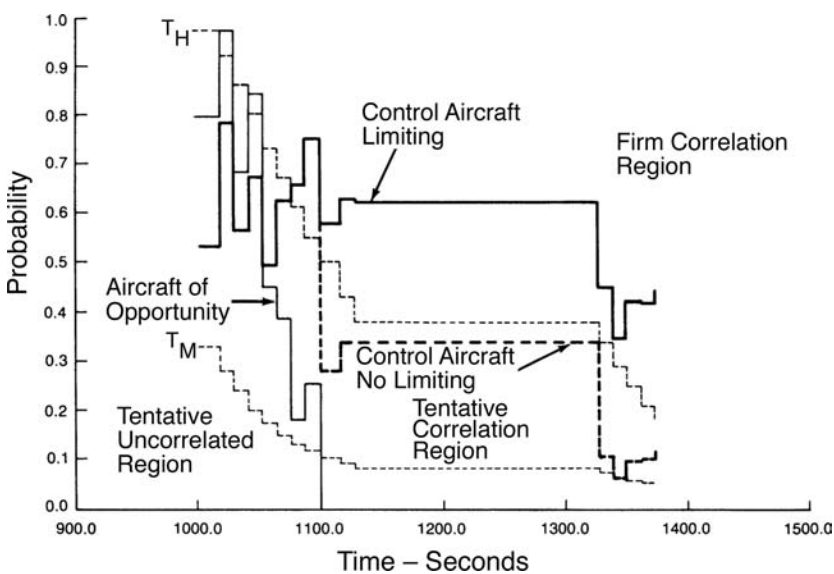

FIGURE 7.45 Association probabilities for experimental data. The bold lines are probabilities for the control aircraft; the solid line, for limiting; the dashed line, for no limiting; the thin line, the association probability for the aircraft of opportunity; and the thin dashed lines, the thresholds T_M and T_H. (*after G.V. Trunk and J.D. Wilson*[80] *© IEEE 1987*)

to multisite operation is straightforward. Specifically, if $\theta_{e1}(t_i)$ and $\theta_{e2}(t_k)$ are the DF angle detections with respect to sites 1 and 2 and if $\theta_{j1}(t_i)$ and $\theta_{j2}(t_k)$ are the estimated angular positions of radar track j with respect to sites 1 and 2, then the multisite squared error is simply

$$d_j = \sum_{i=1}^{n_{1j}} \min\left\{4, [\theta_{e1}(t_i) - \theta_{j1}(t_i)]^2 / {\sigma_1}^2\right\} + \sum_{k=1}^{n_{2j}} \min\left\{4, [\theta_{e2}(t_k) - \theta_{j2}(t_k)]^2 / {\sigma_2}^2\right\} \tag{7.46}$$

The previously described procedure can then be used, with d_j being defined by Eq. 7.46 instead of Eq. 7.45.

REFERENCES

1. J. I. Marcum, "A statistical theory of target detection by pulsed radar," *IRE Trans*., vol. IT-6, pp. 59–267, April 1960.
2. P. Swerling, "Probability of detection for fluctuating targets," *IRE Trans*., vol. IT-6, pp. 269–300, April 1960.
3. J. Neyman and E. S. Pearson, "On the problems of the most efficient tests of statistical hypotheses," *Philos. Trans. R. Soc. London*, vol. 231, ser. A, p. 289, 1933.
4. L. V. Blake, "The effective number of pulses per beamwidth for a scanning radar," *Proc. IRE*, vol. 41, pp. 770–774, June 1953.
5. G. V. Trunk, "Comparison of the collapsing losses in linear and square-law detectors," *Proc. IEEE*, vol. 60, pp. 743–744, June 1972.
6. P. Swerling, "Maximum angular accuracy of a pulsed search radar," *Proc. IRE*, vol. 44, pp. 1146–1155, September 1956.
7. G. V. Trunk, "Survey of radar ADT," Naval Res. Lab. Rept. 8698, June 30, 1983.
8. G. V. Trunk, "Comparison of two scanning radar detectors: The moving window and the feedback integrator," *IEEE Trans*., vol. AES-7, pp. 395–398, March 1971.
9. G. V. Trunk, "Detection results for scanning radars employing feedback integration," *IEEE Trans*., vol. AES-6, pp. 522–527, July 1970.
10. G. V. Trunk and B. H. Cantrell, "Angular accuracy of a scanning radar employing a 2-pole integrator," *IEEE Trans*., vol. AES-9, pp. 649–653, September 1973.
11. B. H. Cantrell and G. V. Trunk, "Corrections to 'angular accuracy of a scanning radar employing a two-pole filter'," *IEEE Trans*., vol. AES-10, pp. 878–880, November 1974.
12. D. C. Cooper and J. W. R. Griffiths, "Video integration in radar and sonar systems," *J. Brit. IRE*, vol. 21, pp. 420–433, May 1961.
13. V. G. Hansen, "Performance of the analog moving window detection," *IEEE Trans*., vol. AES-6, pp. 173–179, March 1970.
14. P. Swerling, "The 'double threshold' method of detection," Project Rand Res. Mem. RM-1008, December 17, 1952.
15. J. V. Harrington, "An analysis of the detection of repeated signals in noise by binary integration," *IRE Trans*., vol. IT-1, pp. 1–9, March 1955.
16. M. Schwartz, "A coincidence procedure for signal detection," *IRE Trans*., vol. It-2, pp. 135–139, December 1956.
17. D. H. Cooper, "Binary quantization of signal amplitudes: effect for radar angular accuracy," *IEEE Trans*., vol. Ane-11, pp. 65–72, March 1964.
18. G. M. Dillard, "A moving-window detector for binary integration," *IEEE Trans*., vol. IT-13, pp. 2–6, January 1967.

19. D. C. Schleher, "Radar detection in log-normal clutter," in *IEEE Int. Radar Conf.*, Washington, DC, 1975, pp. 262–267.
20. "Radar processing subsystem evaluation," vol. 1, Johns Hopkins University, Appl. Phys. Lab. Rept. FP8-T-013, November 1975.
21. H. M. Finn and R. S. Johnson, "Adaptive detection mode with threshold control as a function of spacially sampled clutter-level estimates," *RCA Rev.*, vol. 29, pp. 141–464, September 1968.
22. R. L. Mitchell and J. F. Walker, "Recursive methods for computing detection probabilities," *IEEE Trans.*, vol. AES-7, pp. 671–676, July 1971.
23. G. V. Trunk and J. D. Wilson, "Automatic detector for suppression of sidelobe interference," in *IEEE Conf. Decision & Control*, December 7–9, 1977, pp. 508–514.
24. G. V. Trunk and P. K. Hughes II, "Automatic detectors for frequency-agile radar," in *IEE Int. Radar Conf.*, London, 1982, pp. 464–468.
25. G. V. Trunk, B. H. Cantrell, and F. D. Queen, "Modified generalized sign test processor for 2-D radar," *IEEE Trans.*, vol. AES-10, pp. 574-582, September 1974.
26. J. T. Rickard and G. M. Dillard, "Adaptive detection algorithms for multiple-target situations," *IEEE Trans.*, vol. AES-13, pp. 338–343, July 1977.
27. H. M. Finn, "A CFAR design for a window spanning two clutter fields," *IEEE Trans.*, vol. AES-22, pp. 155–168, March 1986.
28. B. A. Green, "Radar detection probability with logarithmic detectors," *IRE Trans.*, vol. IT-4, March 1958.
29. V. G. Hansen and J. R. Ward, "Detection performance of the cell average log/CFAR receiver," *IEEE Trans.*, vol. AES-8, pp. 648–652, September 1972.
30. G. M. Dillard and C. E. Antoniak, "A practical distribution-free detection procedure for multiple-range-bin radars," *IEEE Trans.*, vol. AES-6, pp. 629–635, September 1970.
31. V. G. Hansen and B. A. Olsen, "Nonparametric radar extraction using a generalized sign test," *IEEE Trans.*, vol. AES-7, September 1981.
32. W. G. Bath, L. A. Biddison, S. F. Haase, and E. C. Wetzlar, "False alarm control in automated radar surveillance systems," in *IEE Int. Radar Conf.*, London, 1982, pp. 71–75.
33. C. E. Muehe, L. Cartledge, W. H. Drury, E. M. Hofstetter, M. Labitt, P. B. McCorison, and V. J. Sferrino, "New techniques applied to air-traffic control radars," *Proc. IEEE*, vol. 62, pp. 716–723, June 1974.
34. G. V. Trunk, "Range resolution of targets using automatic detectors," *IEEE Trans.*, vol. AES-14, pp. 750–755, September 1978.
35. G. V. Trunk, "Range resolution of targets," *IEEE Trans.*, vol. AES-20, pp. 789–797, November 1984.
36. G.V. Trunk and S. M. Brockett, "Range and velocity ambiguity resolution," in *IEEE National Radar Conf.*, Boston, 1993, pp. 146–149.
37. G.V. Trunk and M. Kim, "Ambiguity resolution of multiple targets using pulse-doppler waveforms," *IEEE Trans.*, vol. AES-30, pp. 1130-1137, October 1994.
38. H. Leung, Z. Hu, and M. Blanchette, "Evaluation of multiple radar target trackers in stressful environments," *IEEE Trans. Aerospace and Electronic Systems*, vol. 35, no. 2, pp. 663–674, 1999.
39. B. H. Cantrell, G. V. Trunk, and J. D. Wilson, "Tracking system for two asynchronously scanning radars," Naval Res. Lab. Rept. 7841, 1974.
40. W. D. Stuckey, "Activity control principles for automatic tracking algorithms," in *IEEE Radar 92 Conference*, 1992, pp. 86–89.
41. T. R. Benedict and G. W. Bordner, "Synthesis of an optimal set of radar track-while-scan filtering equations," *IRE Trans.*, vol. AC-7, pp. 27–32, 1962.
42. R. E. Kalman, "A new approach to linear filtering and prediction problems," *J. Basic Eng.* (*ASME Trans.*, ser. D), vol. 82, pp. 35–45, 1960.
43. R. E. Kalman and R. S. Bucy, "New results in linear filtering and prediction theory," *J. Basic Eng.* (*ASME Trans.*, ser. D), vol. 83, pp. 95–107, 1961.

44. S. Blackman and R. Popoli, *Design and Analysis of Modern Tracking Systems*, Boston: Artech, 1999.
45. R. A. Singer, "Estimating optimal tracking filter performance for manned maneuvering targets," *IEEE Trans*., vol. AES-6, pp. 472–484, 1970.
46. B. Friedland, "Optimum steady state position and velocity estimation using noisy sampled position data," *IEEE Trans*. vol. AES, p. 906, 1973.
47. P. Kalata, "The tracking index: A generalized parameter for $\alpha - \beta$ and α, β, γ target trackers," IEEE Trans. Aerospace and Electronic Systems, AES-20, pp. 174–182, 1984.
48. W. D. Blair and Y. Bar-Shalom, "Tracking maneuvering targets with multiple sensors: Does more data always mean better estimates?" *IEEE Trans. Aerospace and Electronic Systems,* vol. 32, pp. 450-456, 1996.
49. F. R.Castella, "Analytical results for the x,y Kalman tracking filter," *IEEE Trans. Aerospace and Electronic Systems*, November 1974, vol. 10, pp.891-894,
50. R. F. Fitzgerald, "Simple tracking filters: Steady-state filtering and smoothing performance," *IEEE Trans. Aerospace and Electronic Systems*, vol. AES-16, pp. 860–864, 1980.
51. G. J. Portmann, J. Moore, and W. G. Bath, "Separated covariance filtering," in *Rec. IEEE 1990 International Radar Conference*, 1990, pp. 456–460.
52. P. Mookerjee and F. Reifler, "Reduced state estimator for systems with parametric inputs," *IEEE Trans. Aerospace and Electronic Systems*, vol. 40, no. 2, pp. 446–461, 2004.
53. A. S. Gelb, *Applied Optimal Estimation*, Cambridge, MA: MIT Press, 1974.
54. F. R. Castella, "Multisensor, multisite tracking filter," *IEE Proc. Radar, Sonar Navigation*, vol. 141, issue 2, pp. 75–82, 1994.
55. E. A. Wan, R. van der Merwe, and A. T. Nelson, "Dual estimation and the unscented transformation," in *Advances in Neural Information Processing Systems 12*, Cambridge: MIT Press, 2000, pp. 666–672.
56. G. A. Watson and W. D. Blair, "IMM algorithm for tracking targets that maneuver through coordinated turns," *SPIE, Signal and Data Processing of Small Targets*, vol. 1698, pp. 236–247, 1992.
57. R. Cooperman, "Tactical ballistic missile tracking using the interacting multiple model algorithm," in *Proc. Fifth International Conference on Information Fusion*, vol. 2, 2002, pp. 824–831.
58. C. L. Morefield, "Application of 0–1 integer programming to multi-target tracking problems," *IEEE Trans*., vol. AC-22, pp. 302–312, 1977.
59. R. Jonker and A. Volgenant, "A shortest augmenting path algorithm for dense and sparse linear assignment problems," *Computing*, vol. 38, no. 4, pp. 325–340, 1987.
60. D. Bertsekas, "The auction algorithm for assignment and other network flow problems: A tutorial," *Interfaces*, vol. 20, pp. 133–149, 1990.
61. I. Kadar, E. Eadan, and R. Gassner, "Comparison of robustized assignment algorithms," *SPIE*, vol. 3068, pp. 240–249, 1997.
62. Y. Bar-Shalom and E. Tse, "Tracking in a cluttered environment with probabilistic data association," *Automatica*, vol. 11, pp. 451–460, 1975.
63. S. B. Colegrove and J. K. Ayliffe, "An extension of probabilistic data association to include track initiation and termination," in *20th IREE Int. Conv. Dig.*, Melbourne, Austrailia, 1985, pp. 853–856.
64. S. B. Colegrove, A. W. Davis, and J. K. Ayliffe, "Track initiation and nearest neighbors incorporated into probabilistic data association," *J. Elec. Electron. Eng. (Australia), IE Aust*. and *IREE Aust*., vol. 6, pp. 191–198, 1986.
65. Y. Bar-Shalom and T. Fortmann, *Tracking and Data Association*, Orlando, FL: Academic Press, 1988.
66. R. W. Sittler, "An optimal association problem in surveillance theory," *IEEE Trans*., vol. MIL-8, pp. 125–139, 1964.
67. J. J. Stein and S. S. Blackman, "Generalized correlation of multi-target track data," *IEEE Trans*., vol. AES-11, pp. 1207–1217, 1975.

68. G. V. Trunk and J. D. Wilson, "Track initiation of occasionally unresolved radar targets," *IEEE Trans*., vol. AES-17, pp. 122–130, 1981.
69. W. Koch, "On Bayesian MHT for well separated targets in densely cluttered environment," in *Proc. IEEE International Radar Conference*, 1995, pp. 323–328.
70. D. J. Salmond, "Mixture reduction algorithms for target tracking in clutter," *SPIE, Signal and Data Processing of Small Targets*, vol. 1305, pp. 434–445, 1990.
71. R. J. Prengaman, R. E. Thurber, and W. G. Bath, "A retrospective detection algorithm for extraction of weak targets in clutter and interference environments," in *IEEE Int. Radar Conf*., London, 1982, pp. 341–345.
72. N. Levine, "A new technique for increasing the flexibility of recursive least squares smoothing," *Bell System Technical Journal*, pp. 819–840, 1961.
73. W. G. Bath, M. E. Baldwin, and W. D. Stuckey, "Cascaded spatial correlation processes for dense contact environments," in *Proc. RADAR 1987*, 1987, pp. 125–129.
74. R. J. Prengaman, R. E. Thurber, and W. G. Bath, "A retrospective detection algorithm for extraction of weak targets in clutter and interference environments," in *IEEE Int. Radar Conf*., London, 1982, pp. 341–345.
75. E. R. Billam, "Parameter optimisation in phased array radar," in *Radar 92*, Brighton, UK, 12–13 October 1992, pp. 34–37.
76. G. V. Trunk, J. D. Wilson, and P. K. Hughes, II, "Phased array parameter optimization for low-altitude targets," in IEEE 1995 International Radar Conference, May 1995 pp. 196–200.
77. W. Bath, "Tradeoffs in radar networking," in *Proc. IEE RADAR 2002*, 2002, pp. 26–30.
78. J. R. Moore and W. D. Blair, "Practical aspects of multisensor tracking," in *Multitarget-Multisensor Tracking: Applications and Advances*, Vol. III, Boston: Artech House, 2000.
79. J. O. Coleman, "Discriminants for assigning passive bearing observations to radar targets," in *IEEE Int. Radar Conf*., Washington, DC, 1980, pp. 361–365.
80. G. V. Trunk and J. D. Wilson, "Association of DF bearing measurements with radar tracks," *IEEE Trans*., vol. AES-23, 1987, pp. 438–447.
81. G. V. Trunk and J. D. Wilson, "Correlation of DF bearing measurements with radar tracks," in *IEEE Int. Radar Conf*., London, 1987, pp. 333–337.